Journal of Archaeological Science 190 (2026) 106551

Contents lists available at ScienceDirect

Journal of Archaeological Science

journal homepage: www.elsevier.com/locate/jas

Spherical harmonic analysis of faceted spheroids identifies shaping strategies and standardisation at Qianshangying (North China)

Zhi Ye [a,b,c], Shuwen Pei [a,b,*], Dongdong Ma [a,b], Hao Li [d,e], Ben Marwick [f,**]

[a] Key Laboratory of Vertebrate Evolution and Human Origins, Institute of Vertebrate Paleontology and Paleoanthropology, Chinese Academy of Sciences, Beijing, 100044, China
[b] Key Scientific Research Base on Paleolithic Human Evolution and Paleogenetics (IVPP), SACH, Beijing, 100044, China
[c] University of Chinese Academy of Sciences, Beijing, 100049, China
[d] Group of Alpine Paleoecology and Human Adaptation (ALPHA), Institute of Tibetan Plateau Research, Chinese Academy of Sciences, Beijing, 100101, China
[e] State Key Laboratory of Tibetan Plateau Earth System, Resources and Environment (TPESRE), Beijing, 100101, China
[f] Department of Anthropology, University of Washington, Seattle, WA, USA

A B S T R A C T

Spheroids are widely distributed lithic artifacts, yet their production strategies and functions remain debated. Traditional morphology-based typologies obscure their technological features and variability. Here we introduce a novel, open-source and reproducible framework that uses spherical harmonics as a method of quantitative morphological analysis, integrated with technological measures, to assess production strategies. Applied to Middle Pleistocene faceted spheroids from Qianshangying (~429 ka, northern China), the approach demonstrates that spheroid production followed a conceptual template, involving a patterned reduction process aimed at achieving standardized spherical forms, and represents a deliberate shaping strategy. Our results further demonstrate that spheroids can be clearly distinguished from polyhedrons and multifacial cores exhausted through reduction. Our methods for investigating spheroid production strategies reveal a higher level of technological complexity than previously assumed for early lithic industries in northern China. Our study also provides a transparent and replicable framework with broad potential for advancing cross-regional and comparative studies of spheroid production but also more broadly for lithic technological research for any period and region.

1. Introduction

Spheroids are a widely distributed type of stone artifact, appearing across a broad temporal and geographic range, from the Oldowan and Acheulean to the Middle Paleolithic, and in diverse archaeological assemblages (Cabanès et al., 2024; Willoughby, 1985). Clark (1955) pioneered the study of archaeological stone balls, then Kleindienst (1962) proposed the sub-divisions of missile, polyhedron and bola. After that, the terminology of spheroid and subspheroid was formally introduced by Leakey (1971) in her classification of the Developed Oldowan. At present, commonly used definitions of ball-like stone artifacts are as follows: spheroids are rounded lithic objects whose entire surface is covered with flake scars, while subspheroids are generally less symmetrical and may retain portions of the original cortex. Compared to spheroids, polyhedrons are characterized by multiple intersecting flake removals, producing a distinctly angular morphology; bolas exhibit smoother and more rounded surfaces with no visible crests (de Weyer, 2017; Leakey, 1971; Titton et al., 2020).

These stone balls are frequently grouped under the category "PSB" of Polyhedron, Spheroid and Bola (or "PSSB" when subspheroids are included) and are commonly interpreted as volumetrically reduced artifacts organized around a central point. This morphology-based classification has been widely accepted, but it has led to challenges. Research has shown that these forms may not represent a continuous *chaîne opératoire*: differences in raw material selection suggest divergent technological strategies and potentially distinct functional purposes (de Weyer, 2017; Jones and others, 1994). This illustrates the limitations of typology in the classification and study of stone artifacts, as it is overly reliant on morphology. There is a need to establish new criteria to distinguish these artifacts and to determine their respective production purposes and strategies, if such purposes and strategies exist.

In addition, the technological category and function of spheroids remain central topics of debate. Broadly, spheroids have been interpreted as cores (Sahnouni et al., 1997), projectiles (Leakey, 1979), and hammerstones (Mussi, 2025; Schick and Toth, 1994), or a specialized tool for working animal bones (Assaf et al., 2025). Closely tied to this

* Corresponding author.
** Corresponding author.
E-mail addresses: peishuwen@ivpp.ac.cn (S. Pei), bmarwick@uw.edu (B. Marwick).

https://doi.org/10.1016/j.jas.2026.106551
Received 25 September 2025; Received in revised form 7 February 2026; Accepted 29 March 2026

debate is the question of their production strategy, which remains unclear. Experimental replication and site-specific diacritical analyses have produced divergent interpretations. One view suggests that spheroids emerged unintentionally as the by-products of core exhaustion, which represents a low-effort strategy aimed at flake production (Sahnouni et al., 1997). Another perspective holds that spheroids were unconsciously produced through high-intensity battering (Clark, 1955; Mora and de La Torre, 2005; Schick and Toth, 1994). In contrast, a third view proposes that spheroids reflect a conceptual template and were produced through a deliberate shaping strategy (Muller et al., 2023; Texier and Roche, 2014; Titton et al., 2020).

This debate remains stalled for several reasons. Typological studies relied heavily on researchers' observations and experiential judgments, which lack objectivity. Some experiments attempted to demonstrate whether spheroids were intentionally or unintentionally produced, yet the researchers involved tend to introduce bias, making it impossible to achieve truly "unconscious" production. From an objective perspective, most studies can only reflect the characteristics of spheroids from a specific region or site, whereas spheroids themselves display considerable diversity in aspects such as raw materials and surface features. Also, conclusions drawn from their own analyses are rarely subjected to external validation or replication. As a result, both the research methods and the inherent diversity of spheroids have hindered the advancement of in-depth studies on spheroids.

To address these challenges, we developed a set of quantitative methods that integrate morphological and technological analyses to investigate spheroid production strategies. While previous morphological measures have focused on the shape of spheroids close to perfect sphere, contributing to discussions of spheroid standardization, they provided limited assistance in reflecting on production strategies. We therefore adopted spherical harmonics, a landmark-free method recently introduced to archaeology. This offers morphometric precision comparable to geometric morphometrics but does not rely on predefined landmarks, making it particularly suitable for artifacts like spheroids that lack homologous landmarks. Compared to previous studies, we employed rotation-invariant spectrum and Uniform Manifold Approximation and Projection to analyze spherical harmonics results, distinguishing the morphological variability of flaked pieces and thereby differentiating spheroids from intensively flaked cores, while extending the application of spherical harmonics. Additional technological analyses, including flake scar orientation analysis and reduction index calculation, further contribute to reconstructing the spheroid production process. All of the methods we present here are open-source to enable replication of our results and support unified, cross-regional quantitative studies in the future.

We demonstrate these methods through a case study of spheroids recovered from the recently excavated site of Qianshangying in the Nihewan Basin, northern China. Using a comparative framework, we examine spheroids alongside polyhedrons and multifacial cores to address two specific questions: first, whether spheroids represent a distinct production sequence, and second whether quantitative methods can distinguish spheroids from heavily reduced cores beyond traditional typological classifications. Further, we situated the Middle Pleistocene Qianshangying site within the broader context of East Asia to explore the technological behaviors and cultural traditions associated with spheroid production, also providing one of the first contributions to understanding the spatial and temporal distribution of spheroids in this region. Finally, and most generally, we offer an efficient and transparent framework combining morphological and technological analyses, enabling comparative studies of spheroid production strategies across regions and archaeological sites that can also be extended to other types of artifacts.

2. Qianshangying and its spheroids

The Qianshangying site complex lies in the Nihewan Basin, a region in northern China situated between the Chinese Loess Plateau and the Inner Mongolian Plateau. The basin preserves extensive Quaternary fluvio-lacustrine and loess deposits (Barbour et al., 1926; Deng et al., 2008; Li et al., 2000; Yuan et al., 2009), hosts the highest concentrations of Pleistocene Paleolithic sites in East Asia, and is especially significant for preserving evidence of early hominin activities outside Africa dating back over one million years (Pei et al., 2017, 2019; Yang et al., 2017, 2020; Zhu et al., 2001, 2004). In recent years, nearly 20 Middle Pleistocene sites—including Jijiazhuang and Caijiagou—have been identified in the southeastern part of the basin (Du et al., 2023; Pei et al., 2018; Ye et al., 2024; Pei et al., 2024), within the Yuxian Sub-basin, resulting in a long and detailed regional cultural sequence for the Nihewan Basin (Fig. 1).

The Qianshangying site complex consists of four localities from QSY-A to QSY-D, discovered in 2015. It is among the region's most artifact-rich archaeological sites. Geomorphological and sedimentological evidence indicates that the stratigraphy at the site records a full cycle of lake expansion, retreat, re-expansion, and eventually disappearance of the ancient Nihewan lake, and hominin occupation occurred in a marginal lacustrine setting during a low lake-level episode (Deng et al., 2008; Li, 2020; Ye et al., 2025b, 2024; Yuan et al., 2009; Zhou et al., 1991). The stratigraphic context of Qianshangying indicates a short-term occupation resulting from a single hominin activity event. Analyses of artifact orientations and size distributions indicates that the assemblage appears to be largely *in situ*, exhibiting minimal disturbance after deposition (Ye et al., 2025b). ESR dating of the cultural layer places hominin activity at approximately 429 ± 39 ka (Ye et al., 2025b).

A total of 955 stone artifacts were recovered from four localities at Qianshangying. Following a widely used techno-typological framework (de la Torre, 2004; de la Torre and Mora, 2018; Isaac, 1981, 1986; Pei et al., 2017) (The numerical distribution and proportional composition of these categories are provided in the supplementary material), the distinction between spheroids and other lithic categories was independently assessed by two researchers. Spheroids and subspheroids are all faceted stone tools with intensive flake scars on the surface. Compared to multifacial cores and polyhedrons, spheroids and subspheroids are characterized by more rounded edges rather than sharp angles, consistent with our consensus definition of near-spherical forms. Within this continuum, spheroids show a more symmetrical morphology and more extensive flake scar coverage, while subspheroids are characterized by lower symmetry and a less intensive degree of shaping. A spheroid group of 13 artifacts were identified, including 6 spheroids and 7 subspheroids, accounting for 1.3% of the total lithic assemblage. Multifacial cores and polyhedrons are intensively flaked cores with more than three flaking surfaces, with polyhedrons generally regarded as approaching spherical forms (de la Torre, 2011). In this study, artifacts with a thickness-to-length ratio greater than 0.6 are operationally classified as polyhedrons (n = 17), as these specimens tend to exhibit more comparable dimensions along the three principal axes, whereas the remaining pieces are classified as multifacial cores (n = 12). Importantly, this classification reflects a morphological continuum rather than discrete categories; the threshold value of 0.6 is adopted as a practical criterion to distinguish polyhedrons from multifacial cores, producing roughly comparable sample sizes for the two categories within the assemblage.

Raw materials at Qianshangying were classified into four categories following Pei and Hou (2002) and Pei et al. (2017): lava, dolomite, chert, and others. The overall assemblage is dominated by lava (n = 637, 66.7%), followed by dolomite (n = 209, 21.9%), with smaller proportions of chert (n = 53, 5.5%) and other materials (n = 56, 5.9%). The composition of cores closely mirrors this distribution, among them, polyhedrons and multifacial cores show higher frequency on chert (n = 3, 10.3%) and lower frequency on dolomite (n = 5, 17.2%). In contrast, spheroids and subspheroids exhibit a marked preference for lava (n = 11, 84.6%), with reduced use of siliceous dolomite (n = 2, 15.4%) and no use of chert. Compared to the cores, spheroids and subspheroids show a stronger reliance on lava and a diminished use of

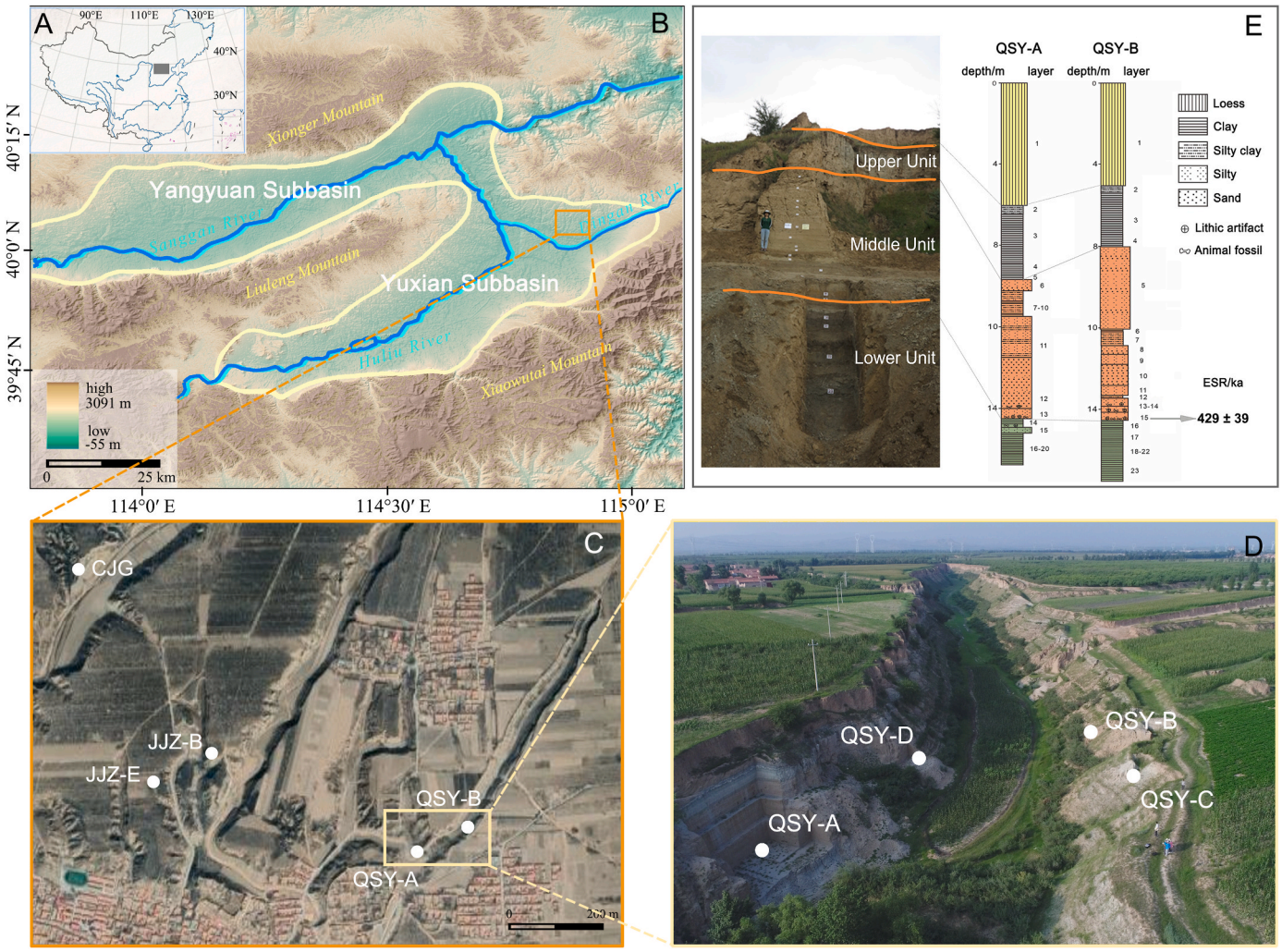

Fig. 1. Geological Context and Chrono-Stratigraphy of the Qianshangying site complex): A-B) Geographic location of Nihewan basin. C) Google Earth image showing major sites in the Jijiazhuang Platform. D) Landscape and different localities of Qianshangying site complex. E) Archaeostratigraphic sequence and ESR dating results of Qianshangying site.

more fragile materials, suggesting a selective strategy favoring raw materials with more stable and homogeneous physical properties.

In terms of dimensions, the average length, width, thickness, and mass of spheroids and subspheroids were 81.9 mm (SD = 30.7), 72.3 mm (SD = 29.7), 63.8 mm (SD = 26.1), and 660 g (SD = 755.6), respectively, as shown in Fig. 2. Few spheroids and subspheroids showed outlier values in size, being either unusually large or small, while the rest exhibited relatively concentrated size distributions. Polyhedrons and multifacial cores displayed similar even lower variability in size and weight. However, spheroids and subspheroids tend to have similar values across length, width, and thickness, reflecting their overall symmetry. Polyhedrons and multifacial cores show marked differences

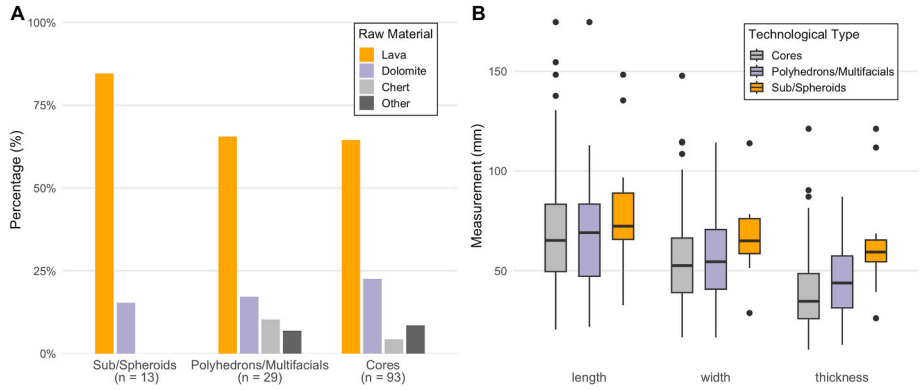

Fig. 2. Basic characteristics of the Qianshangying assemblage. A: Raw material proportions. B: Box plot comparing basic metric dimensions of cores, subspheroids/spheroids, and polyhedra/multifacial cores.

among these dimensions, indicating more irregular and elongated forms.

3. Methods

We generated 3D models of the cores for morphometric and technological analysis. Digital data were captured using Artec Spider, and post-processing was carried out with Artec Studio 18. Methods and indicators used in this research are generally listed in supplementary material files methods_and_indicators_outline.xlsx. The 3D scan files and all the R (4.4.3) and Python (3.10.2) code used in the analyses reported here are openly available online at https://doi.org/10.17605/OSF.IO/CTNE9/.

3.1. Morphometric analysis

In our morphometric study, we used quantitative methods including the sphericity index, spherical harmonics with spherical harmonic energy (SHE) to show the shape features of spheroids and subspheroids. We assessed the degree of standardization of spheroids and subspheroids by calculating the coefficients of variation (CVs) of shape proxies, defined as the sample standard deviation divided by the sample mean (Eerkens and Bettinger, 2001; Muller and Clarkson, 2023) of shape proxies. Following Eerkens and Bettinger (2001), a CV below 1.7% (0.017) was taken as threshold of standardized manual production. Furthermore, we compared the results of the typological classification and our new morphometric analyses.

3.1.1. 3D spherical harmonics analysis

Spherical Harmonic (SPHARM) analysis is a method for describing 3D shapes using a series of mathematical functions defined on the surface of a sphere. It works like a 3D version of Fourier analysis, breaking down complex shapes into components of different spatial frequencies. Each shape $f(\theta,\phi)$ is first mapped onto a unit sphere and then expressed as a combination of spherical harmonic basis functions $Y_l^m(\theta,\phi)$ according to

$$f(\theta,\phi)=\sum_{l=0}^{\infty}\sum_{m=-l}^{l}\widehat{f}(l,m)Y_l^m(\theta,\phi)$$

where the set of coefficients $\widehat{f}(l,m)$ quantifies how much each basis function contributes to the overall shape. Here, θ and ϕ are angles in spherical coordinates, l and m are order and degree respectively. Lower-order terms describe the general shape, while higher-order terms capture finer details (Fig. 3).

This method has been widely used in the field of biology, for example in the analysis of skull and cell morphology (Grieb et al., 2022; Harper et al., 2022; Hewitt et al., 2024; Link et al., 2024; Medyukhina et al., 2020). In contrast, archaeological applications of SPHARM remain limited and have followed a small number of distinct methodological pathways, including the use of SPHARM-based point distribution models to establish surface correspondence for asymmetry assessment (e.g. Sholts et al. (2017)), the application of spherical harmonics to test hypotheses of intentionality in lithic reduction (e.g. Muller et al. (2023)), and the construction of empirical morphospaces via PCA of SPHARM coefficients for descriptive shape analysis (e.g. Noshita et al. (2025)). Despite demonstrating the potential of SPHARM for archaeological materials, these studies commonly focus on descriptive interpretations of spherical harmonic coefficients or their principal components, and are largely confined to linear dimensionality reduction frameworks, which may limit the exploration of high-resolution or non-linear structure in shape variation. Moreover, open and fully reproducible analytical workflows are still rarely implemented in archaeological applications of SPHARM.

Our work builds on previous archaeological applications of SPHARM to present an open-source and fully reproducible workflow for quantitative shape analysis of stone artifacts. We extend existing approaches by combining rotation-invariant spherical harmonic power spectrum with non-linear dimensionality reduction using Uniform Manifold Approximation and Projection (UMAP), enabling feature-based exploration and unsupervised grouping of spheroids and cores, which

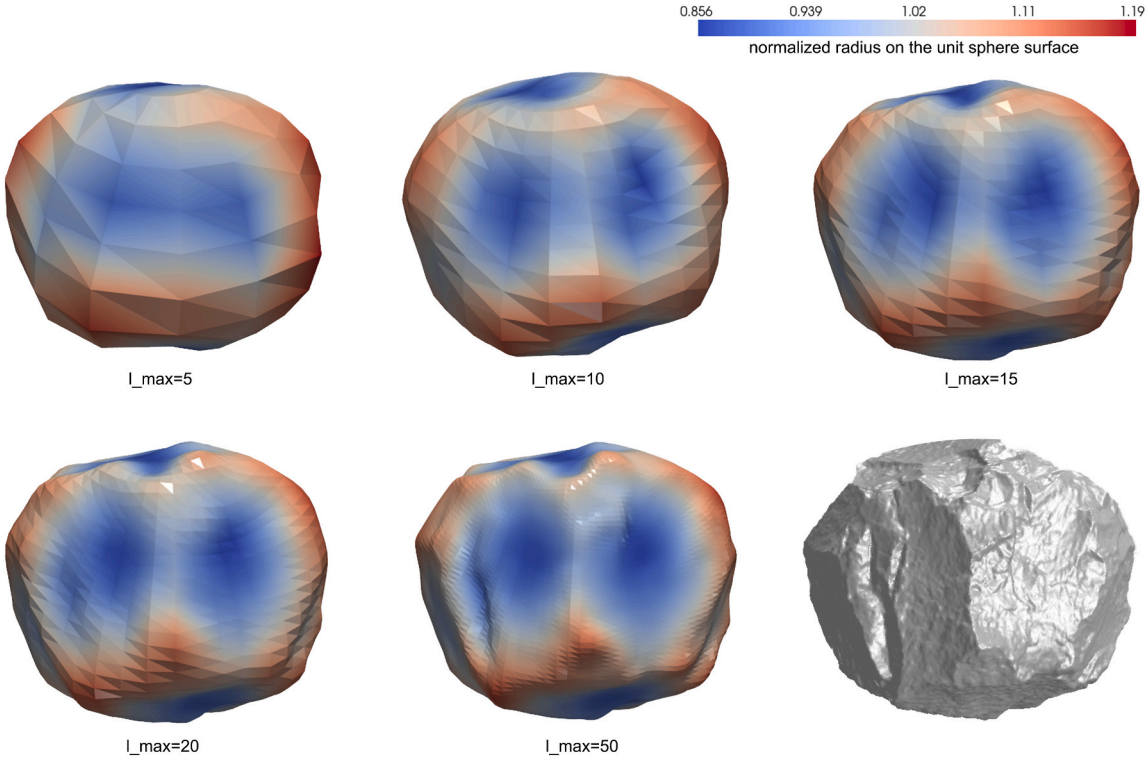

Fig. 3. Shape reconstruction of selected archaeological spheroids using SPHARM (various lmax levels).

substantially extends the depth of analysis provided by SPHARM.

As shown in Fig. 4, following Medyukhina et al. (2020) and Link et al. (2024), scanned models of spheroids and cores were imported, cleaned, simplified, and normalized to obtain 3D mesh vertices. These vertices were converted from Cartesian (x, y, z) to spherical coordinates (r, θ, φ), and radial values were interpolated onto a regular N × N spherical grid. Spherical harmonic decomposition was then performed using the Driscoll–Healy sampling scheme (Wieczorek and Meschede, 2018), setting the maximum degree to 20 (lmax = 20, Fig. 3). This choice ensures that sufficient geometric detail is captured while avoiding high-frequency noise and overfitting artifacts. After normalization, all models have their degree 0 (l = 0) coefficient set to 1, allowing for meaningful comparison across different models.

From the normalized spherical harmonic coefficients, we computed the rotation-invariant power spectrum by summing the squared magnitudes of coefficients at each degree, yielding a multidimensional and orientation-independent shape descriptor for each model. Using these rotation-invariant power spectrum as input, we applied UMAP for nonlinear dimensionality reduction and visualization (Bavel et al., 2023), preserving both local and global similarity structure in the shape data. Clusters in the resulting UMAP space were identified using K-means clustering, providing a quantitative basis for grouping spheroids, polyhedra, and multifacial cores. To aid interpretation of the morphospace and cluster assignments, a set of standard geometric reference models (sphere, rounded cube, ellipsoid, rounded box, and disc-like forms) were included in the analyses, allowing artifacts to be positioned relative to these reference shapes and facilitating morphological interpretation of groupings based on both cluster membership and shape similarity. The data acquisition related to SPHARM was all carried out using Python.

3.1.2. Spherical harmonic energy and sphericity index

We computed the spherical harmonic energy (SHE), defined as the sum of squared normalized spherical harmonic coefficients for each degree. This provides a rotation-invariant measure of overall shape complexity and surface regularity. For normalized shapes, this total energy approaches a value of one for a perfect sphere, while more irregular shapes yield higher values.

We also employed a standardized sphericity index originally proposed by Wadell (1935) and later adapted for 3D digital models in geoscientific research. The index is calculated using volume and surface area of the artifact. This dimensionless metric yields a maximum value of 1 for a perfect sphere. While values closer to 1 generally indicate a more spherical geometry, sphericity is calculated solely from volume and surface area. We used Python to derive surface area and volume measurements from 3D mesh models.

The classic sphericity index (Wadell, 1935) may exhibit limitations in differentiating morphotypes with equivalent surface-area-to-volume ratios. SHE supplements this by performing spherical harmonic decomposition of surface morphology, and this allows it to distinguish localized irregularities (like core edge or concave) from global shape

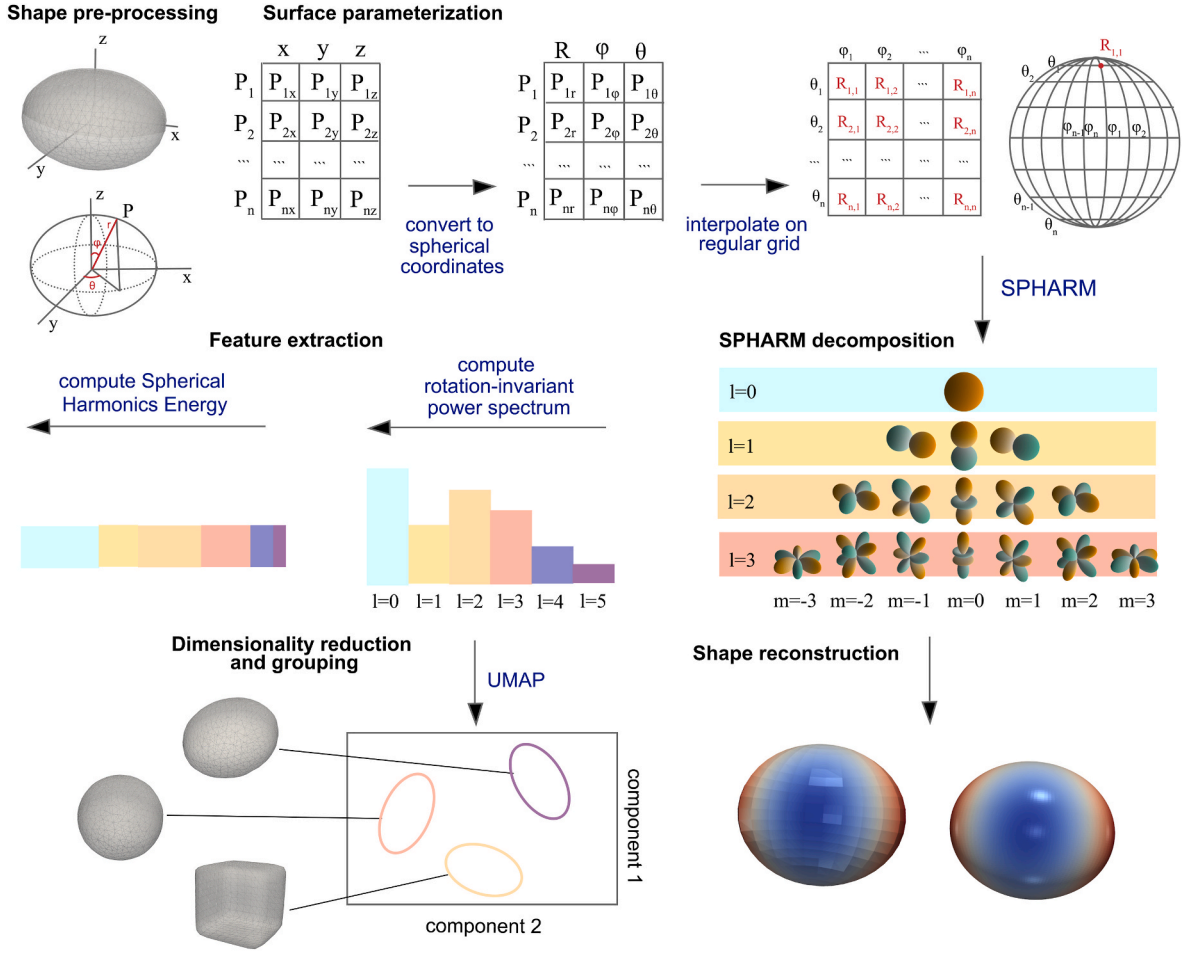

Fig. 4. Schematic summary of the key steps of 3D spherical harmonics analysis. First, raw 3D scans of stone artifacts are processed by mapping their surface points onto a standardized spherical grid. The object's complex geometry is then mathematically decomposed into a series of fundamental shape components (Spherical Harmonics), ranging from general forms to fine details. From this decomposition, we extract numerical fingerprints of the shape, specifically the rotation-invariant power spectrum and total energy, which allow for objective comparison regardless of the object's orientation. Finally, these quantitative features are used to statistically cluster similar artifacts into groups (using UMAP) and to visually reconstruct shape models for interpretation.

deviations (e.g., elongation)-differences that classic sphericity index metrics often fail to capture.

3.2. Technological analysis

We applied technological analysis of the production strategies of spheroids and subspheroids in Qianshangying (Grieb et al., 2022; Link et al., 2024). Together these methods help determine whether the artifacts were intentionally shaped and whether their manufacture followed standardized procedures. Addressing this question is crucial for achieving our goal of determining whether or not spheroids and subspheroids represent a distinct technological category, separate from exhausted cores.

3.2.1. Diacritical analysis

We used diacritical analysis to reconstruct the reduction sequence based on superimposition relationships among scars on spheroids and subspheroids (Cabanès et al., 2024; Titton et al., 2020). This method enables the identification of the order of scar removal, allowing us to understand the organization of removals. All spheroids and subspheroids were included in the analysis to assess whether their removal were organized systematically.

Following the reconstruction of reduction sequences, we adopted an inductive approach to infer exploitation models of spheroids, that is, the removal patterns and associated stages employed in a spheroid. If consistent patterns can be observed, they may indicate shared reduction schemes or conceptual templates.

3.2.2. Orientation analysis

This method derives from fabric analysis originally used in sedimentology and has since been adapted to study the arrangement of flake scars on lithic artifacts. We followed the protocol developed by Lin (2024). In our study, only those scars with a length greater than 5 mm were recorded, after extracting scar vectors from each samples and calculating eigenvalues we computed the isotropic ratio and elongation ratio and visualized the result in a ternary plot. These steps were carried out in Geomagic Wrap 2021, Rhino8 and R 4.4.3 and documented in Ye et al. (2025a).

Results were visualized using ternary plots to compare orientation statistics between spheroids and other core types. Based on our hypothesis, if spheroids were shaped following a consistent reduction sequence, they should exhibit similar and patterned orientation results. In contrast, if they merely represented exhausted cores, the orientation patterns would appear random and highly variable, similar to those of undirected polyhedron and multifacial cores.

3.3. Efficiency of shaping strategy

The following method aims to test a hypothesis regarding reduction strategy. We propose that knappers may have employed an efficient shaping strategy directed toward achieving a spherical form. If such a strategy existed, then across the assemblage of final products, we should observe that as reduction intensity increases, spheroid morphology progressively approximates a perfect sphere. To test this hypothesis, we established two sets of quantitative proxies: one for inferred reduction intensity and another for final morphology. Specifically, a significant positive correlation between these two sets of proxies would support the inference that increased reduction intensity was systematically associated with shapes closer to a sphere, implying a goal-directed reduction strategy.

3.3.1. Intensity of reduction

To compute the degree of reduction we collected data on three metrics: scar number, removal ratio and scar density index (SDI). We measured scar number as total number of flake scars visible on the spheroid surface. Removal ratio was calculated as 1 minus cortex ratio, where the cortex ratio represents the proportion of cortical surface area to total surface area (Cabanès et al., 2024). We used the removal ratio instead of the traditional cortex ratio in order to maintain a positive correlation with other reduction intensity indicators. The scar density index (SDI), defined as the number of flake scars divided by the total surface area, serves as a robust indicator of core reduction intensity, effectively capturing the dynamic nature of the reduction process (following Clarkson (2013)). In all three metrics, higher values represent more advanced stages of reduction. Scar counts and surface area measurements were extracted using Geomagic Wrap.

3.3.2. Spheroid shape

We measured spheroid shape with four metrics: sphericity index, and spherical harmonic energy (SHE), along with mean edge angle, and mean surface curvature. To assess mean edge angle, ten edge intersections were randomly sampled on each spheroid, and edge angles were calculated following Titton et al. (2020) by constructing triangles at ridge intersections, extracting vertex coordinates in Geomagic Wrap, and computing the angles from these coordinates using trigonometric functions in R. Higher mean edge angles indicate a more spherical geometry. We estimated local curvature for each triangular face of the 3D mesh model using a k-nearest neighbors approach in Python. For each triangle, a best-fit plane was fitted to its neighboring triangle centers, and the angle between the triangle's normal and the best-fit plane's normal was computed. The average of these angles across all triangles was served as mean surface curvature and quantified overall surface roughness, with larger values indicating greater roughness. Together, these four variables allowed us to assess whether more extensively reduced spheroids display more standardized, symmetrical, and regular morphologies—characteristics expected in deliberate shaping strategies.

We conducted Spearman's rank correlation analysis between two sets of variables, reduction intensity indicators and morphological attributes. This non-parametric method is appropriate for small sample sizes and data that do not follow a normal distribution. Spheroids and subspheroids from Qianshangying were included in the analysis.

4. Results

4.1. Morphometric analysis

Table 1 summarizes the basic information (rock type, blank type and final morphology) and morphological analysis results (classifications derived from SPHARM, values for sphericity and spherical harmonic energy) of the spheroids, subspheroids, polyhedra and multifacial cores involved in the research (see Table 2).

Sphericity results reveal no significant difference between multifacial cores and polyhedrons (a Wilcoxon rank-sum test yielding $W = 268$, $p = 2.76 \times 10^{-2}$). Accordingly, for subsequent analysis, we combined these two into a single group, which was then compared with the group of spheroids and subspheroids. A clear difference is shown between the group of spheroids and subspheroids and the group of polyhedrons and multifacial cores. The mean sphericity of spheroids (0.91) is notably higher than that of polyhedrons and multifacial cores (0.86, panel C Fig. 5), with a Wilcoxon rank-sum test yielding $W = 100$, $p = 2.54 \times 10^{-10}$. This result indicates that spheroids and subspheroids possess a more spherical geometry overall, supporting their typological classification as a distinct type.

Subsequently, we computed the rotation-invariant power spectrum. Here we present the power spectrum of different groups, including the group of spheroids and subspheroids, group of polyhedrons and multifacial cores, and the total of all these categories combined (panel A Fig. 5). The results show that the spheroids and subspheroids have significantly lower power than polyhedrons and multifacial cores at both low and high degrees, indicating that spheroids and subspheroids possess a more symmetrical overall shape and more regular local

Table 1
Summary of core typology and morphological parameters.

ID	Rock_type	Blank type	Final morphology	Typology	typology by SPHARM	Sphericity	SHE
QSY_A_0256	Lava	Cobble	Polyhedral	Polyhedron	Ellipsoid or box	0.866	1.020
QSY_A_0562	Other-quartz	Nodule	Cubical	Multifacial	Discoid-like	0.827	1.043
QSY_A_0570	Lava	Cobble	Cubical	Multifacial	Discoid-like	0.826	1.080
QSY_A_0576	Lava	Flake	Pyramidal	Polyhedron	Discoid-like	0.809	1.050
QSY_A_0579	Chert	Nodule	Pyramidal	Multifacial	Discoid-like	0.799	1.054
QSY_A_0680	Chert	Nodule	Pyramidal	Multifacial	Discoid-like	0.803	1.039
QSY_A_0682	Lava	Cobble	Polyhedral	Subspheroid	Sphere or rounded cube	0.917	1.010
QSY_A_0699	Lava	NA	Cubical	Multifacial	Discoid-like	0.881	1.025
QSY_A_0700	Other-quartzite	Cobble	Pyramidal	Polyhedron	Sphere or rounded cube	0.893	1.017
QSY_A_0702	Lava	Cobble	Pyramidal	Polyhedron	Discoid-like	0.842	1.042
QSY_A_0735	Lava	Cobble	Pyramidal	Polyhedron	Sphere or rounded cube	0.868	1.020
QSY_A_0938	Lava	NA	Pyramidal	Polyhedron	Discoid-like	0.869	1.027
QSY_A_1098	Lava	NA	Rounded	Spheroid	Ellipsoid or box	0.919	1.013
QSY_A_1111	Chert	Nodule	Pyramidal	Polyhedron	Ellipsoid or box	0.872	1.023
QSY_A_1246	Lava	Nodule	Polyhedral	Subspheroid	Sphere or rounded cube	0.893	1.011
QSY_A_1304	Lava	Cobble	Pyramidal	Polyhedron	Sphere or rounded cube	0.927	1.013
QSY_A_1307	Dolomite	Nodule	Cubical	Multifacial	Discoid-like	0.868	1.037
QSY_A_1333	Lava	NA	Cubical	Multifacial	Discoid-like	0.861	1.031
QSY_A_1517	Lava	Flake	Pyramidal	Multifacial	Discoid-like	0.796	1.075
QSY_A_1584	Lava	NA	Pyramidal	Polyhedron	Sphere or rounded cube	0.855	1.019
QSY_A_1777	Dolomite	Cobble	Rounded	Spheroid	Sphere or rounded cube	0.897	1.011
QSY_A_1941	Lava	Cobble	Polyhedral	Subspheroid	Sphere or rounded cube	0.901	1.011
QSY_A_2048	Lava	Cobble	Cubical	Polyhedron	Discoid-like	0.891	1.030
QSY_A_2049	Lava	Cobble	Pyramidal	Multifacial	Discoid-like	0.869	1.031
QSY_A_2213	Lava	NA	Polyhedral	Subspheroid	Sphere or rounded cube	0.878	1.011
QSY_A_2381	Lava	Cobble	Pyramidal	Multifacial	Ellipsoid or box	0.876	1.028
QSY_A_2599	Lava	Cobble	Polyhedral	Polyhedron	Ellipsoid or box	0.902	1.017
QSY_A_2600	Dolomite	Cobble	Rounded	Spheroid	Sphere or rounded cube	0.927	1.010
QSY_A_2611	Dolomite	Nodule	Polyhedral	Polyhedron	Discoid-like	0.820	1.040
QSY_A_2717	Lava	Cobble	Polyhedral	Subspheroid	Sphere or rounded cube	0.905	1.011
QSY_A_2723	Lava	Cobble	Rounded	Spheroid	Sphere or rounded cube	0.907	1.009
QSY_A_2797	Lava	NA	Rounded	Spheroid	Sphere or rounded cube	0.938	1.004
QSY_B_003	Lava	Cobble	Rounded	Spheroid	Sphere or rounded cube	0.915	1.015
QSY_B_072	Lava	Cobble	Polyhedral	Subspheroid	Ellipsoid or box	0.902	1.020
QSY_B_136	Lava	Cobble	Polyhedral	Polyhedron	Ellipsoid or box	0.879	1.019
QSY_B_140	Dolomite	Nodule	Polyhedral	Polyhedron	Discoid-like	0.886	1.024
QSY_B_159	Lava	Cobble	Pyramidal	Polyhedron	Discoid-like	0.863	1.024
QSY_B_168	Lava	Cobble	Cubical	Multifacial	Ellipsoid or box	0.899	1.024
QSY_B_186	Dolomite	Nodule	Polyhedral	Polyhedron	Discoid-like	0.869	1.027
QSY_B_189	Lava	Cobble	Cubical	Subspheroid	Ellipsoid or box	0.905	1.016
QSY_B_320	Lava	Cobble	Cubical	Multifacial	Discoid-like	0.859	1.053
QSY_B_435	Dolomite	Nodule	Cubical	Polyhedron	Ellipsoid or box	0.858	1.020

Table 2
Summary of spheroid shaping intensity and shape features. SDI = scar density index, SHE = spherical harmonic energy.

ID	Scar number	Removal ratio	SDI	Mean edge angle	Curvature	Sphericity	SHE
QSY_A_0682	10	0.837	0.000	123.585	9.220	0.917	1.010
QSY_A_1098	29	0.973	0.003	128.338	7.998	0.919	1.013
QSY_A_1246	31	0.921	0.003	123.936	8.090	0.893	1.011
QSY_A_1777	14	0.927	0.005	122.208	7.979	0.897	1.011
QSY_A_1941	8	0.681	0.001	109.423	9.902	0.901	1.011
QSY_A_2213	26	0.922	0.002	114.985	8.873	0.878	1.011
QSY_A_2600	22	0.852	0.001	124.385	7.145	0.927	1.010
QSY_A_2717	20	0.860	0.001	122.426	8.954	0.905	1.011
QSY_A_2723	27	0.918	0.001	134.926	8.275	0.907	1.009
QSY_A_2797	28	0.960	0.002	135.403	7.453	0.938	1.004
QSY_B_003	14	0.647	0.000	120.931	6.750	0.915	1.015
QSY_B_072	4	0.623	0.000	115.484	8.008	0.902	1.020
QSY_B_189	15	0.782	0.001	117.941	7.626	0.905	1.016

features. In addition, the spheroid and subspheroid group exhibits smaller inter-group morphological variation than polyhedrons and multifacial cores, particularly at low degrees. Then we performed a Variance Analysis on the power of each harmonic degree. The results indicate that $l = 2$ and $l = 3$ exhibit the highest variance across the sample (panel B Fig. 5), suggesting that these low-degrees capture the most significant shape variation. Specifically, $l = 2$ reflects elongation or flattening, while $l = 3$ reflects a sphere with octupole (pear-shaped) deformation exhibits a triaxial asymmetry that departs from both spherical and ellipsoidal symmetry.

The spherical harmonic energy (SHE) demonstrates significant negative correlation with classic sphericity index ($r = -0.83$, $df = 82$, $p = 6.82 \times 10^{-23}$), validating its efficacy as a proxy for how closely an object approximates a spherical form (panel D Fig. 5). Statistical comparisons reveal distinct SHE distributions between groups: spheroids and subspheroids exhibit a mean SHE of 1.012, whereas multifacial cores and polyhedra demonstrate significantly higher irregularity (mean SHE = 1.033) (panel C Fig. 5). The Wilcoxon rank-sum test confirms

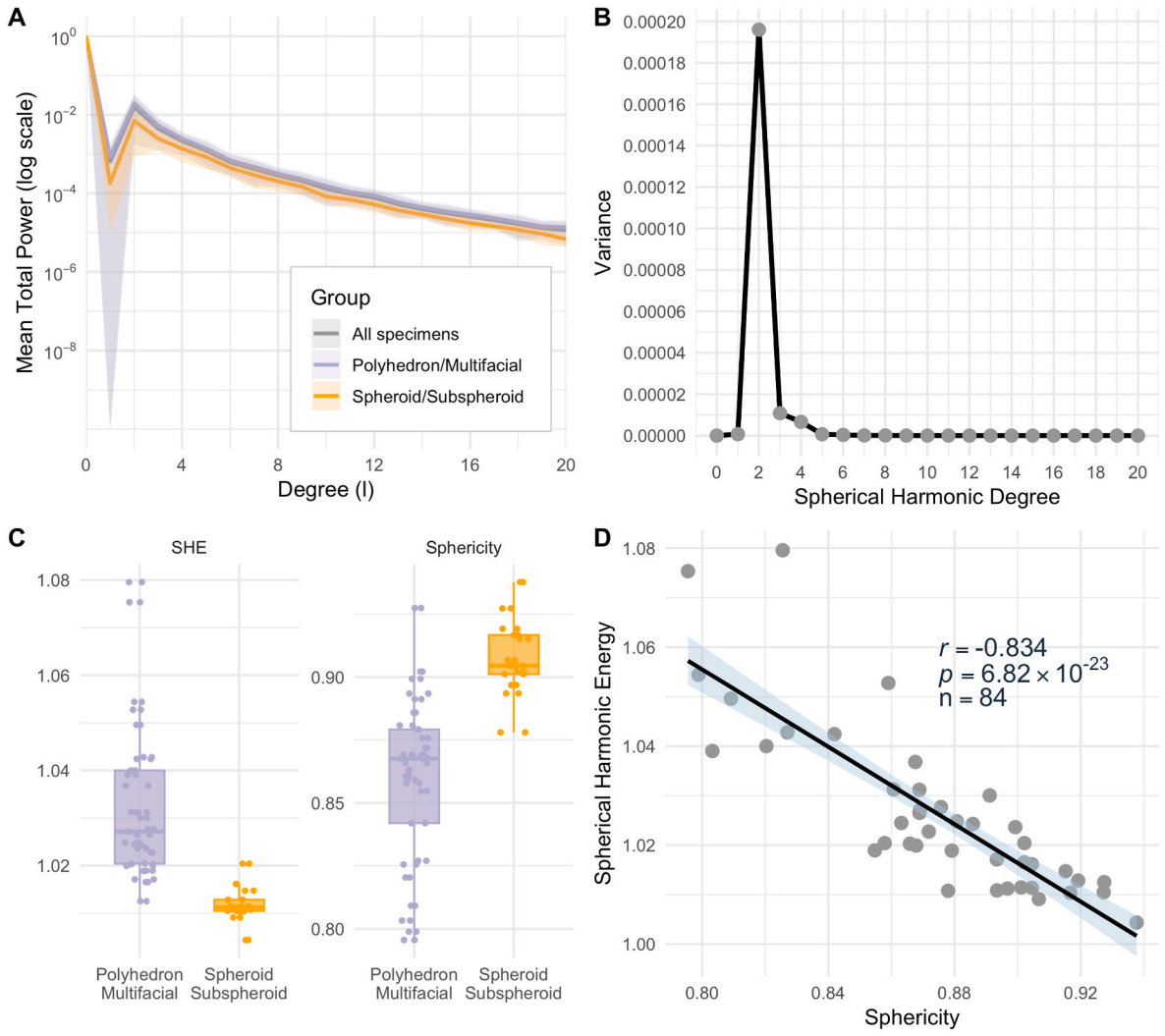

Fig. 5. A. Mean spherical harmonic power spectrum. B. Variance distribution by spherical harmonic degree. C. Distribution of SHE and sphericity by artifact type. D. Correlation of sphericity and spherical harmonic energy(r refers to the correlation coefficient; p refers to the p-value; n refers to the sample size).

robust inter-group divergence ($W = 1468$, $p = 5.05 \times 10^{-12}$), confirming the distinguishability of spheroid and subspheroid group from Qianshangying.

The pursuit of a standardized and distinct spherical form among spheroids and subspheroids is supported by Coefficient of Variation (CV). Both sphericity and SHE values yielded low CVs of under 1.7% (0.017 and 0.004, respectively), indicating that group of spheroids and subspheroids maintain a highly standardized rounded shape (panel C Fig. 5). In contrast, the group of multifacial cores and polyhedron has a higher CV of 0.038 and 0.016 respectively.

We then applied a Uniform Manifold Approximation and Projection (UMAP) to the rotation-invariant power spectrum, followed by K-means clustering to identify and characterize distinct morphological groups. The result reveals distinct clusters in the first two dimensions of the shape space. These clusters correspond to reference models of sphere, rounded cube, ellipsoid, rounded box and disc-like (Fig. 6). This demonstrates that these flaked pieces occupy distinguishable regions in the shape space, with proximity to the sphere or elongation or flattening along specific axes emerging as key differentiating features. Most artifacts typologically classified as spheroids or subspheroids were grouped into the "sphere" and "rounded cube", and few into "ellipsoid" and "box" clusters, indicating their consistent, near-spherical shapes (Fig. 6).

However, a few Multifacial cores and Polyhedra also appeared in the near-spherical region. This can be attributed to their high cortex coverage or limited flake removals, which likely preserved their originally rounded shapes and led to their grouping alongside spheroids. Some artifacts are identified as spheroids or subspheroids but grouped as ellipsoid or rounded box, because they exhibit a long axis. This reflects the use of different classification criteria in typological and quantitative approaches: typological assessments consider artifacts close to spherical, particularly when they exhibit large edge angles and rounded surfaces, whereas spherical harmonic analysis emphasizes aspects such as absolute symmetry.

The UMAP-based groupings correspond to significant differences in sphericity, as indicated by a Kruskal–Wallis test ($\chi^2 = 40.35$, df = 2, $p = 1.73 \times 10^{-9}$). The result shows statistically significant differences in sphericity among the shape clusters, further supporting the effectiveness of the spherical harmonic approach in capturing meaningful morphological variation.

4.2. *Technological analysis*

Diacritical analysis of spheroid and subspheroid surfaces reveals a structured and recurrent reduction sequence comprising three phases (Fig. 7). Phase one was a unidirectional or bidirectional total exploitation, belonging to one kind of volume exploitation. Large and flat surfaces of the cobble were selected as platforms for striking toward the opposite surface. Knapping proceeded until the peripheral volume was

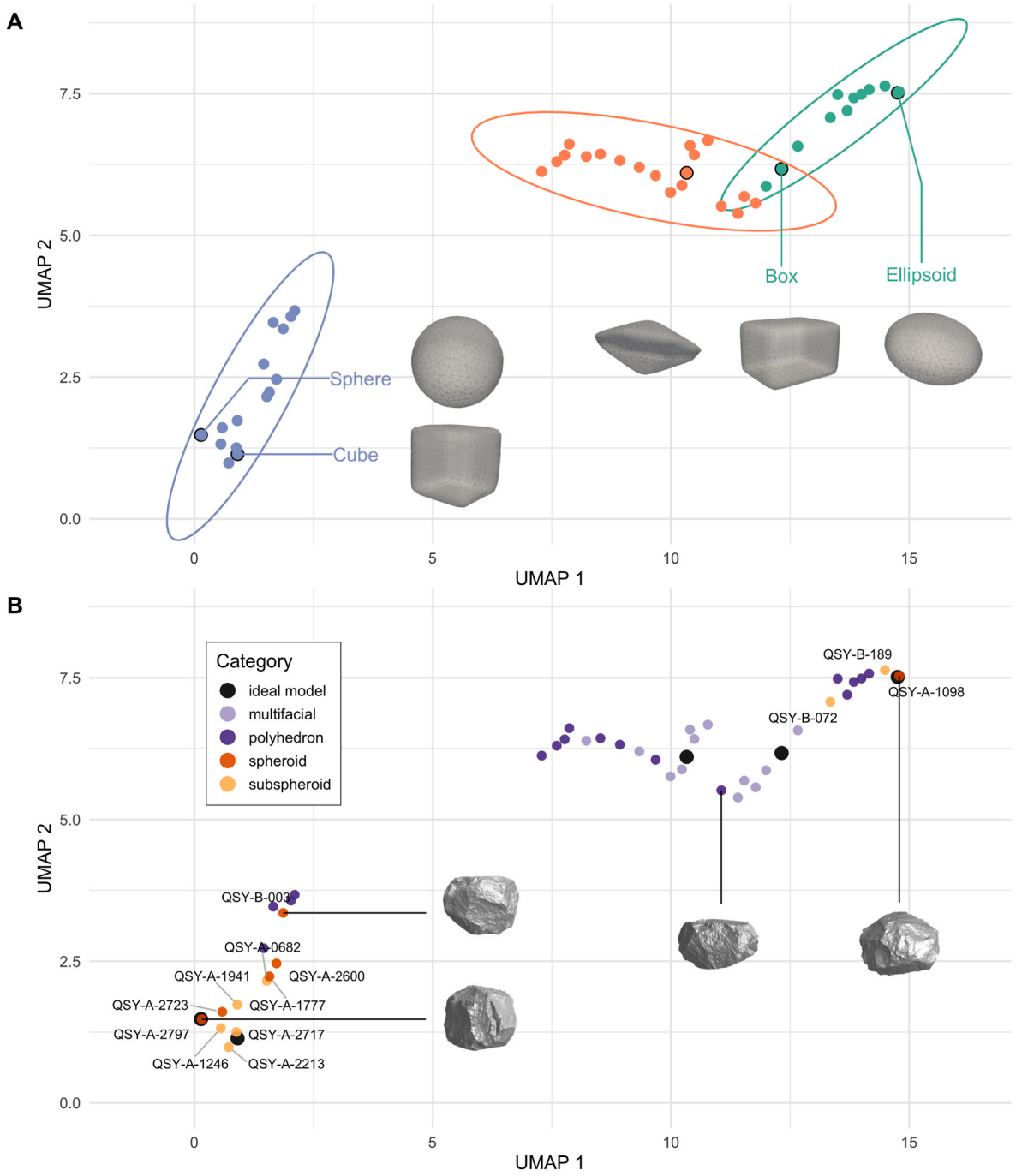

Fig. 6. A. UMAP plot showing distinct clusters of shapes derived from SPHARM. B. UMAP plot of SPHARM-derived shape features colored by types. UMAP plot axes represent relative positions in a reduced-dimension morphospace and do not have a direct physical interpretation.

fully exploited, resulting in an approximately cubic form. Phase two was peripheral centripetal exploitation. In this phase, previous removals in phase one serve as platforms for centripetal flaking around the core periphery. This represents a surface exploitation stage. A notable feature is the angle between the flaking surface and platform (i.e. core edge angle), which often exceeds 90°. This phase contributes significantly to the increasingly spherical shape of the artifact. Phase three was the production of small scars on ridges or intersections of previous flake scars, resulting in a rounding surface, further enhancing roundness.

At the Qianshangying site, all spheroids fall within Phase 3 of the reduction sequence, with one specimen appearing to have skipped Phase 2 and proceeded directly to edge refinement. In contrast, subspheroids display greater variability in their reduction sequences: Four specimens are assigned to Phase 3, of which two appear to have skipped Phase 2; one specimen falls within Phase 2, and one specimen within Phase 1 (see supplementary material files spheroids_metrics.xlsx). However, one subspheroid bypassed Phase 1 and instead employed a strategy of bifacial centripetal exploitation combined with edge refinement. Notably, in this case the angle between the two flaking surfaces approaches 90°, distinguishing this subspheroid from typical discoid cores. This suggests that the purpose of reduction was not the production of flakes, but rather the direct shaping of the artifact into its final spherical form. Also, it is important to note that due to the high degree of reduction intensity observed in some spheroids, phases prior to the visible sequence were often obliterated. We hypothesize the existence of a Phase zero, potentially involving roughing-out of the cobble or an

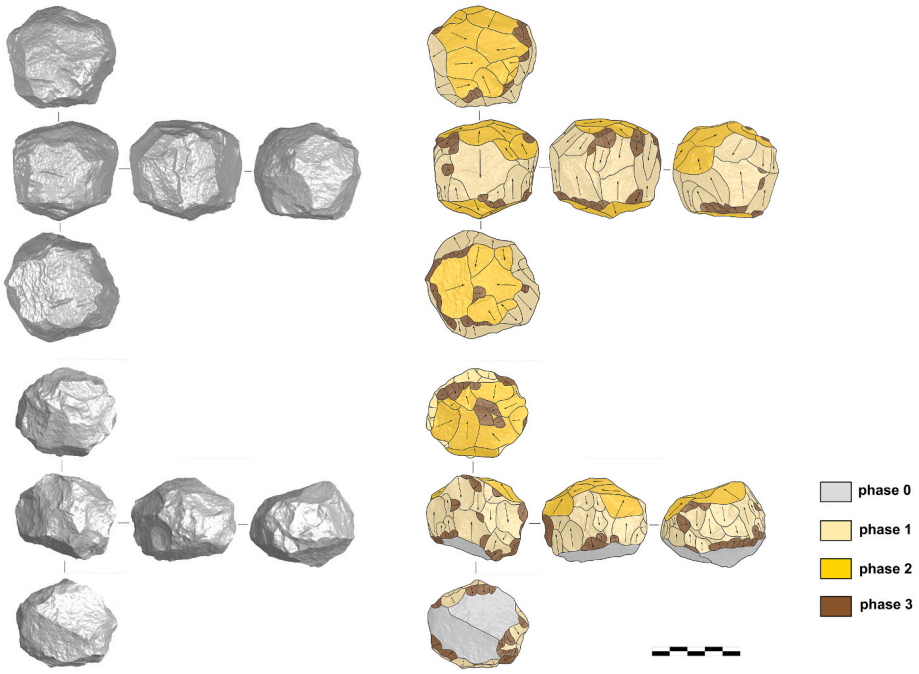

Fig. 7. Diacritical analysis of Qianshangying spheroids.

earlier cycle of Phases one to three Fig. 8.

Scar orientation analysis further supports the interpretation of a systematic reduction sequence in the production of Qianshangying spheroids and subspheroids. Fig. 9 shows that spheroids tend to cluster together, with elongation ratios ranging from 0.403 to 0.634 and isotropy ratios from 0.182 to 0.497. These elongation ratios suggest that the spheroids underwent unidirectional or bidirectional total exploitation, typical of Phase one, resulting in relatively high elongation values. Then the peripheral centripetal exploitation, namely Phase two, appears to have contributed to a certain degree of isotropy in scar orientation, and higher isotropy ratios are associated with more spherical forms. Subspheroids exhibit greater variability in both elongation and isotropy ratios, reflecting less standardized reduction than spheroids. They remain more morphologically clustered than multifacial cores and polyhedra, though this distinction is subtle.

Multifacial cores and polyhedra display a wide and dispersed distribution in the ternary plot, without forming any distinctive cluster. Their scar patterns show considerable variability in both elongation and isotropy, reinforcing the interpretation that these cores lack removal organization. Multifacial cores typically exploit natural angles with core rotation occurring without a fixed plan, while polyhedra, despite showing a higher degree of reduction, follow a similarly various flaking sequence. This distinction highlights the fundamental technological difference between group of polyhedrons and multifacial cores and group of spheroids at Qianshangying. While they used to be considered as a continuous reduction process, our results show that in fact polyhedra and multifacial cores represent exhausted cores, whereas the spheroid and subspheroid group reflects the presence of a distinct conceptual template and systematic reduction plan.

4.3. *Shaping strategy efficiency*

For group of spheroids and subspheroids, we conducted shaping efficiency analysis.The same analysis was conducted on group of polyhedrons and multifacial cores as a comparison. Fig. 10 shows the results. Among reduction intensity descriptors, removal ratio and SDI incorporate surface area in their calculation, making them more effective in capturing the density and intensity of reduction, and therefore more comparable indicators of the reduction process compared to scar number.

Among the shape descriptors, we observed several significant correlations in the group of spheroids and subspheroids. Mean edge angle was positively correlated with sphericity ($\rho = 0.68$, $p = 0.010$) and negatively correlated with Spherical Harmonics Power (SHE)

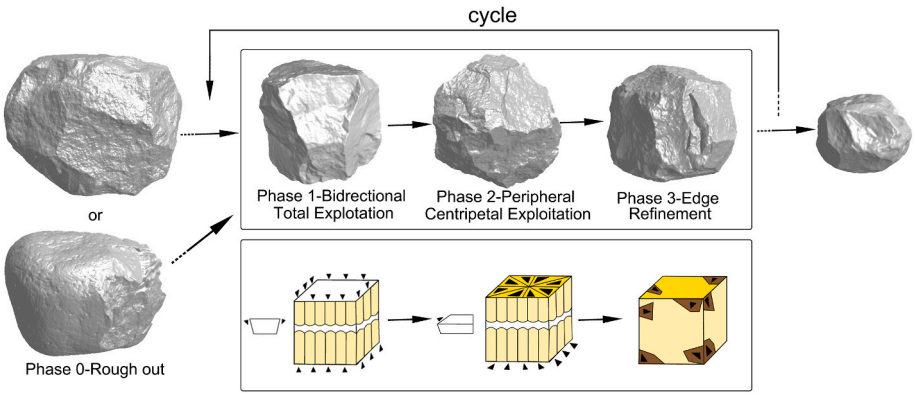

Fig. 8. Hypothetical spheroid shaping process at Qianshangying.

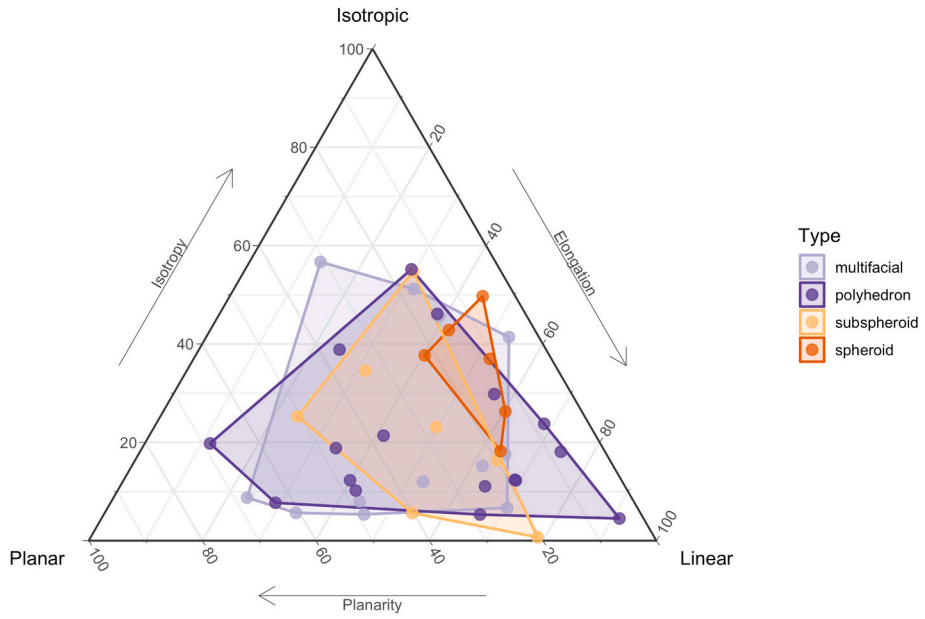

Fig. 9. Ternary plot showing flake scar orientation analysis.

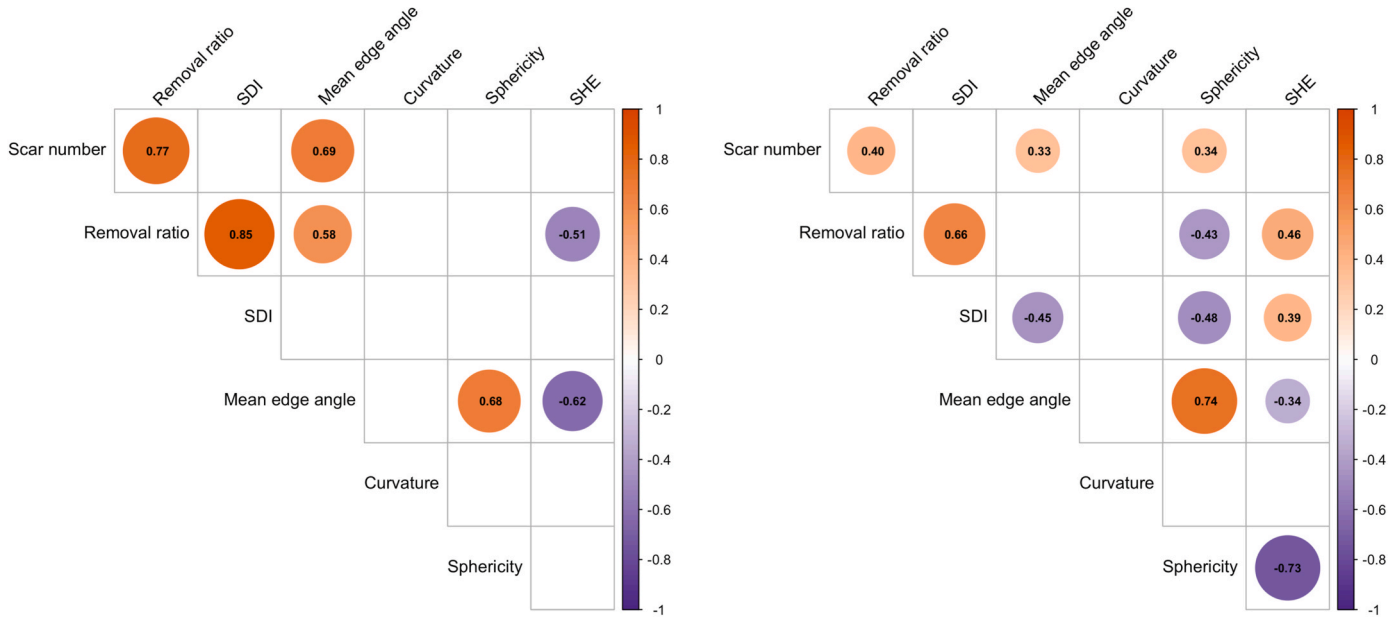

Fig. 10. Spearman correlation matrix of shape variables. Left: Spheroids and subspheroids. Right: Polyhedrons and multifacial cores. Circle indicates $p < 0.1$, with size representing correlation magnitude. Non-significant correlations ($p \geq 0.1$) are shown without circles.

($\rho = -0.62$, $p = 0.024$), indicating that greater edge angles are associated with more spherical and regular forms. Curvature was not significantly correlated with other variables, which may reflect its focus on local surface texture, while edge angle, sphericity and SHE capture broader aspects of shape regularity and symmetry. The weak correlation between sphericity and SHE may result from the small sample size or their different sensitivities: sphericity, based on area and volume, tolerates surface variation, while SHE responds more to asymmetry and shape irregularity. Thus, even in specimens with similar sphericity, surface differences can produce substantial variation in SHE. The analysis of spheroid shape variables indicates that mean edge angle, curvature, sphericity, and SHE each capture distinct aspects of spheroid morphology, which explains the varying strengths of correlation observed among them.

Significant correlations were found between removal ratio and mean edge angle in the group of spheroids and subspheroids. Mean edge angle was positively correlated with both scar number ($\rho = 0.69$, $p = 0.010$) and removal ratio ($\rho = 0.58$, $p = 0.037$). SHE showed a negative correlation trend with removal ratio ($\rho = -0.51$, 0.074). Although this correlation did not reach the conventional significance threshold of $p < 0.05$, likely due to the small sample size, the relatively strong Pearson correlation suggests this negative relationship warrants attention. These results suggest that as reduction progresses, spheroids develop larger edge angles and lower SHE.

However, no significant correlations were observed between reduction intensity variables and sphericity or curvature. This implies that increased reduction does not necessarily produce smoother surfaces. Such patterns likely reflect the technological nature of the samples: the

analyzed spheroids and subspheroids are "faceted" products of flake removal. Flaking increases surface complexity by adding edges and angular intersections, which may elevate curvature while also expanding surface area, factors that can distort sphericity values.

In contrast, the polyhedra and multifacial core group exhibits a distinct morphological trajectory: higher core reduction intensity correlated with lower sphericity and higher SHE values. This pattern suggests that sustained flaking activity in polyhedral cores leads to increasingly irregular forms that deviate from spherical geometry. This comparative analysis allows us to address our initial research question: spheroids or subspheroids do not represent a product of intensive flaking in the same manner as polyhedra.

5. Discussion

5.1. Do the Qianshangying spheroids represent a shaping strategy?

According to the results of technological analysis, we can summarize the technical strategy employed in the production of faceted spheroids and subspheroids from Qianshangying. This strategy consists of a series of sequential phases (Fig. 8): a potential rough-out phase, volume exploitation aimed at forming a symmetrical cubic shape, surface exploitation to approximate a spherical geometry, edge refinement, and potentially the repetition of earlier phases. The existence of a repetitive phase is supported by the observation that while the original cobble blanks from Qianshangying display considerable size variation, the finished spheroids, although few of them are relatively large or small, mostly cluster around a diameter of 6–9 cm (Fig. 2). This suggests that the production of spheroids may have involved multiple cycles of reduction, and further implies that a diameter of 6–9 cm was considered an optimal or intended size in the knapping process.

The symmetrical and standardized shape of spheroids and subspheroids is observed in Qianshangying. The observed relationships between reduction intensity and shape descriptors support the interpretation that spheroid shaping was an efficient and purposeful process. The goal was to produce well-structured, globally spherical spheroids rather than smooth objects. By comparing group of spheroids and subspheroids and group of polyhedrons and multifacial cores, we can conclude that while spheroids must undergo significant reduction to achieve their near-spherical morphology, conversely, not all exhausted cores acquire spherical morphology.

Therefore, our results indicate that the Qianshangying hominins deliberately employed a standardized production approach to create spheroids with consistent and formalized shapes. The technological strategy reflected in the Qianshangying faceted spheroids and subspheroids includes the use of a conceptual template, standardized production, and the achievement of a target product, which together demonstrate that this was a shaping strategy. This stands in contrast to flaking strategies, where the primary objective is the removal of useable flakes rather than the shaping of a cobble into a predetermined morphology (Duke et al., 2021; Inizan et al., 1999).

These findings also contribute to the long-standing debate over the nature of spheroids–whether they should be interpreted as byproducts of flake production, or as targeted end products of shaping strategies. In the case of the Qianshangying faceted spheroids and subspheroids, the evidence strongly supports the latter. Faceted spheroids recovered from other Early Pleistocene sites in Barranco Leon and 'Ubeidiya have also been reported to show evidence consistent with shaping strategy (Muller et al., 2023; Titton et al., 2020). These intentionally shaped spheroids appear contemporaneous with, or even predate, the emergence of Acheulean technology, which is commonly considered the hallmark of the formalization of shaping strategies.

It is important to note, however, that many spheroids from East Africa may not fall into this category. As noted by Mora and de La Torre (2005), these quartz spheroids may have been produced through percussive techniques. They are often covered with battering marks, exhibit smoother surfaces and lack ridges, features that suggest they may be better classified as bolas within a typological framework (Leakey, 1971). It may be more appropriate to describe these artifacts in technological terms, rather than relying on morphology-based typologies that can lead to confusion. For instance, referring to them as battering spheroids could help distinguish them from faceted spheroids.

Another question our results are relevant to is the relationship between polyhedrons, spheroids, and bolas. While no bolas were identified at Qianshangying, our quantitative analyses clearly differentiated polyhedrons from spheroids or subspheroids. These two artifact types differ in size, morphology, and production sequence. Polyhedrons at Qianshangying represent heavily reduced cores, whose edge angle increase results from extensive flake removal. Their primary purpose lies in producing flakes, placing them within a flaking strategy. In contrast, spheroids and subspheroids were intentionally shaped as end products, reflecting a shaping strategy. These two technological approaches of flaking and shaping strategies coexisted at Qianshangying, indicating a diversity of reduction goals.

However, we found that although the morphology and reduction technology of spheroids and polyhedrons can be clearly distinguished, spheroids in early phases may be difficult to differentiate from cores. In their initial phases of reduction, spheroids often resemble cores due to similar flake removal patterns. At this stage, they may be classified as cores, especially since the flakes produced during the initial shaping are themselves useable. As Cabanès et al. (2022) mentioned, they could share a common operative chain before completing the final product. However, it remains unclear whether this typological transformation was intentional or unplanned.

5.2. Qianshangying spheroids in the context of East Asia

In East Asia, spheroids constitute a technological category with broad temporal and spatial distribution (Yi et al., 2012), as shown in Fig. 11 (see the supplementary materials for a table of more information about these sites). In addition to the one spheroid collected near the Gongwangling site in Shaanxi (Dai and Xu, 1973), the earliest dated spheroids originate from Zhoukoudian Locality 1 (ZKD Loc.1) (Nanjing Institute of Geology and Palaeontology, Chinese Academy of Sciences, 1985), attributed to the early Middle Pleistocene, and not far from Qianshangying. In terms of geographic range, the southernmost and westernmost occurrences of spheroids are found at the Mujiaqiao site (MJQ) in Yunnan (Wei et al., 1984), while the northernmost spheroids come from the Jinsitai site (JST) in Inner Mongolia (Wang et al., 2010). The widespread occurrence of spheroids across time and space in East Asia may indicate their role as a generalized or multipurpose tool within Pleistocene contexts, capable of serving diverse functions in varying ecological and cultural settings.

Over 1522 spheroids have been identified across more than 23 archaeological sites or localities in East Asia. However, many of these findings derive from surface surveys rather than systematic excavations, and the recovered quantities are often limited. Thus, the number of spheroids per site varies considerably: 19 sites have yielded fewer than ten specimens each. Qianshangying is typical with six spheroids and seven subspheroids. By contrast, three sites—Xujiayao (XJY), Dingcun (DC), and JST—have produced substantial assemblages, each exceeding 100 spheroids (Shanxi Provincial Institute of Archaeology, 2014; Wang, 2016; Wang et al., 2010). Notably, XJY alone has yielded over 1000 specimens (Wang, 2016).

The raw materials used for spheroids at these archaeological sites primarily include quartz, quartzite, sandstone, and limestone, with occasional occurrences of lava and dolomite at a few localities, such as Qianshangying. Among these, quartz and quartzite are the most widely used materials, found at 18 sites across China. In contrast, spheroids made of sandstone and limestone are mainly concentrated at sites distributed along the Fen River and Li River basins in Central China. Previous researches have observed that the morphological

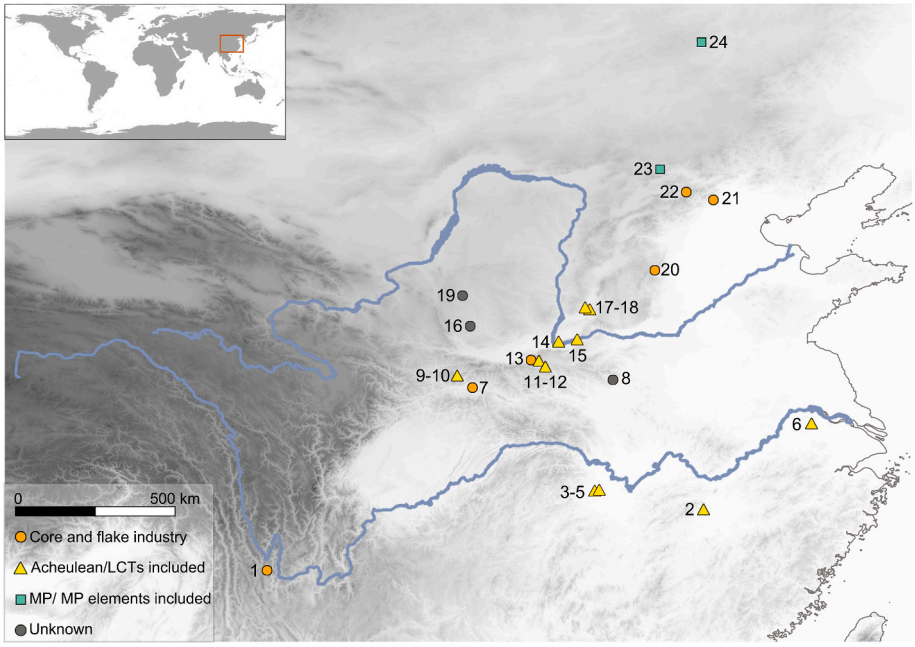

Fig. 11. Map of Paleolithic Sites with Spheroids in China and Their Associated Lithic Industries. 1. Mujiaqiao, (Wei et al., 1984); 2. Liaohe river region, (Li and Xu, 1991); 3. Deshan Second Brick factory, (Xi, 1994); 4. Zhangjiatan, (Lixian County Museum, 1992); 5. Huzhua Mount., (Tan, 1999); 6. Fangniu Mount., (Fang et al., 2002); 7. Fanba, (Xia et al., 2022); 8. Xiaokongshan, (Xiaokongshan Joint Excavation Team, 1988); 9. Hejialiang, (Wang et al., 2014); 10. Longgangsi, (Lu et al., 2006); 11. Shangdan basin, (Wang et al., 2013); 12. Yaoshi basin, (Wang and Hu, 2000); 13. Choushuihe, (Dai and Xu, 1973); 14. Kehe, (Jia, 1962); 15. Shuigou, (Huang, 1964); 16. Hezhigou, (Liu et al., 1984); 17. Xigou, (Jia, 1959); 18. Dingcun, (Shanxi Provincial Institute of Archaeology, 2014; Tao et al., 1984); 19. Liujiacha, (Xie, 1982); 20. Dangcheng, (Wu and Sun, 1989); 21. Zhoukoudian Loc.1, (Nanjing Institute of Geology and Palaeontology, Chinese Academy of Sciences, 1985); 22. Qianshangying, (Ye et al., 2025b); 23. Xujiayao (Jia et al., 1979; Jia and Wei, 1976; Ma et al., 2011; Wang, 2016); 24. Jinsitai (Wang et al., 2010).

characteristics of spheroids are influenced by the physical properties of the raw materials (Tao et al., 1984). For example, at the DC site, spheroids made from quartz tend to be irregular and angular, possibly due to the fragile nature of quartz. In comparison, those made from softer materials such as limestone and sandstone are generally more rounded and smoother, with flake scars that appear more diffuse or less distinct (Tao et al., 1984).

Three primary techniques have been identified in the manufacture of spheroids in China: flaking, involving the removal of flakes to shape the object (e.g., Qianshangying, MJQ, Wei et al., 1984); pecking, where two blanks are struck together to round off edges, sometimes by splitting a cobble and using the halves against each other (e.g., DC, Shanxi Provincial Institute of Archaeology, 2014); and battering, involving repeated percussion of a polyhedrons (e.g., ZKD Loc.1, Nanjing Institute of Geology and Palaeontology, Chinese Academy of Sciences, 1985). Experimental studies suggest that pecking and battering yield similar efficiency and spherical form (Lu et al., 2021). Many sites, such as XJY and DC, show evidence of multiple techniques, including combined or sequential methods like pecking after flaking to improve roundness (Nanjing Institute of Geology and Palaeontology, Chinese Academy of Sciences, 1985; Tao et al., 1984). No clear relationship has yet been established between raw material types and specific production methods.

We found six sites exhibiting similar strategies to Qianshangying. For example, at DC and MJQ, thick and flat cobbles were selected and shaped through peripheral flaking, producing roughly approximately cubic shape (Tao et al., 1984; Wei et al., 1984). MJQ specimens retain parts of the cortex, while at DC, flakes with large exterior and small interior platform angles were removed from blanks to increase edge angles and enhance roundness (Tao et al., 1984; Wei et al., 1984). Among the six sites, all but MJQ are located within the Fen River and Lishui River regions. These sites were grouped into the Keheng–Dingcun techno-complexes and Lishui techno-complexes, characterized by trihedral picks (Fang et al., 2002; Jia, 1962; Lixian County Museum, 1992; Shanxi Provincial Institute of Archaeology, 2014; Tan, 1999). The trihedral picks were produced by striking the dorsal surfaces of large flakes to concentrate edges at the tip, resulting in triangular outlines and robust pointed ends, classifying them as large cutting tools (LCTs) (Kuman et al., 2014; Li et al., 2018; Yang et al., 2016). This is a significant observation, as it implies that spheroid production techniques similar to those at Qianshangying are more frequently associated with lithic assemblages characterized by intentional shaping strategies.

It should be emphasized, however, that we do not intend to imply a direct association between faceted spheroids and Acheulean technology. We infer that faceted spheroids in China appear to represent a shaping tradition that shares the same crucial technological competencies as LCTs (Cabanès et al., 2024; Isaac, 1986; Leakey, 1971), and this could explain why they often occur in Acheulean techno-complex. We now find that faceted spheroids and subspheroids occur at Qianshangying within the context of a small flake tool industry. This industry, based on a core and flake technology, has been attributed to Mode 1 in north China. The presence of faceted spheroids, however, suggests that this technocomplex was more complex and exhibited greater variability than previously thought.

Similarly, we may need to reconsider the technological complexity implied by faceted spheroids. Faceted spheroids appear in what is considered the Late Oldowan, if a chronological boundary is set at 2.0 Ma to distinguish between Early and Late Oldowan (Gallotti et al., 2018). The growing recognition of technological diversity within the Oldowan has led to a broader consensus that the Late Oldowan includes signs of innovation, such as more complex flaking patterns and decreased morphological variability in flakes (Braun et al., 2019; Gallotti et al., 2018). Faceted spheroids, we propose here, may represent one of the key indicators of this increasing technological complexity during the Late Oldowan (Titton et al., 2020).

6. Conclusions

Quantitative approaches to studying spheroids remain limited (de Weyer, 2017; Muller et al., 2023; Titton et al., 2020). We propose a complete, efficient, reproducible and transparent methodological framework here based on spherical harmonics to quantitatively assess morphological variation among flaked pieces, allowing for the distinction between cores and spheroids and evaluating the degree of morphological standardization in spheroids. Past approaches to analyzing the morphology of flaked pieces have been limited, with geometric morphometrics being the most recent major method innovation (Cao et al., 2025; Hallinan and Cascalheira, 2025; Lycett and Von Cramon-Taubadel, 2013). However, this method has significant constraints, including the requirement for homologous landmarks, which limits its applicability to artifacts like cores of various shapes and spheroids. Spherical harmonics offer a viable alternative, showing strong potential for precision and interpretability. We can reasonably expect broader applications of this method across a wide range of archaeological artifacts in the future.

In principle, any closed three-dimensional object can be analyzed using spherical harmonics. In archaeology, materials such as spheroids or cores, ceramic vessels, plant seeds, and animal crania are particularly well suited to this approach, as their overall forms approximate spheres or ellipsoids, making them readily mappable onto the unit sphere for spherical harmonic expansion. Low-order expansions efficiently capture their primary morphological features, while the combination of low-order and high-order coefficients allows for a distinction between overall shape (e.g., symmetry, inflation, elongation) and local details (e.g., decorations, ridges, protrusions). Moreover, these objects generally do not emphasize orientation, enabling the use of rotationally invariant spherical harmonic power spectrum to quantify shape variation. For objects with weaker symmetry or greater surface complexity, however, higher-order expansions are required, increasing computational cost and complicating the interpretation of coefficients. As a tool for morphological research, spherical harmonics are particularly effective in addressing issues of shape symmetry and standardization (Grieb et al., 2022; Muller et al., 2023). Moreover, owing to the high precision of spherical harmonic decomposition, they offer significant advantages in investigating morphological variation both within and between groups (Link et al., 2024; Medyukhina et al., 2020; Noshita et al., 2025).

By applying a range of quantitative methods, we conducted an integrated morphological and technological study of the Qianshangying spheroids. Our results demonstrate that these spheroids were produced through a programmed reduction strategy aimed at achieving standardized spherical forms, primarily using hard-hammer direct percussion. The evidence of shaping strategies on Qianshangying spheroids even subspheroids confirms that they were intentionally made tools with conceptual template, rather than exhausted cores. This distinguishes them from polyhedrons or multifacial cores in their terminal reduction stages. Traditionally, lithic technology in northern China prior to the Late Pleistocene has been considered stagnant and generally classified as simple core and flake industry. However, the Qianshangying assemblage from ~429ka clearly reveals a higher level of technological complexity.

This paper also presents one of the first systematic overviews of the spatial and temporal distribution and technological variability of spheroids within East Asia. We found that East Asian spheroids display considerable diversity in raw materials, production techniques, and morphology. Some assemblages contain spheroids that may be comparable to those from Qianshangying and tend to appear within Acheulean or shaping-oriented techno-complexes, often dated later than Qianshangying. This highlights the particular significance of the Qianshangying spheroids and subspheroids. However, the current dataset remains limited, and many sites lack detailed morphological and technological studies of spheroids, hampering broader inferences about hominin technological behaviors. We therefore emphasize the need for site-specific analysis of spheroids in future research.

Given the limitations of traditional typology in capturing the functional, morphological, and technological variability of spheroids across sites, we argue that multiple method approaches are essential. From the perspective of typology, spheroids have often been dismissed as poor marker of hominin behavior due to their wide spatial and temporal distribution. However, more recent studies increasingly reveal their diversity and potential as markers of hominin technological behavior (Cabanès et al., 2024; de Weyer, 2017; Titton et al., 2020; Vaquero and Romagnoli, 2018). For example, distinctions between flaking-based and battering-based spheroids, along with patterns of raw material selection, production goals, and associations with specific subsistence strategies or environmental adaptations, may prove meaningful and need further explore(Cabanès et al., 2024). Beyond the methods of morphological and technological analysis used here, future studies incorporating functional analysis and experimental replication will also enhance our understanding of spheroid manufacture, a specific production activity.

Reproducible results

The Associate Editor for Reproducibility could download all materials and reproduce the results presented by the authors.

Data availability statement

The 3d models from Qianshangying and the Python and R code and used to analyse these models for this study are openly available at https://doi.org/10.17605/OSF.IO/CTNE9.

Funding

This work was financially supported through the National Natural Science Foundation of China (Grant No. 42371165), and China Scholarship Council Programme for international students (CSC No. 202404910542).

CRediT authorship contribution statement

Zhi Ye: Conceptualization, Data curation, Investigation, Methodology, Software, Writing – original draft. **Shuwen Pei:** Investigation, Resources, Supervision, Writing – review & editing. **Dongdong Ma:** Investigation, Writing – review & editing. **Hao Li:** Data curation, Supervision, Writing – review & editing. **Ben Marwick:** Data curation, Methodology, Supervision, Writing – review & editing.

Declaration of competing interest

The authors declare that they have no known competing financial interests or personal relationships that could have appeared to influence the work reported in this paper.

Acknowledgements

Thanks to Christine Harper for kindly sharing her expertise on SPHARM analyses.

Appendix A. Supplementary data

Supplementary data to this article can be found online at https://doi.org/10.1016/j.jas.2026.106551.

References

Assaf, E., Pérez, S.D., Bruner, E., Torres, C., Blasco, R., Rosell, J., Preysler, J.B., 2025. The use of shaped stone balls to extract marrow: a matter of skill? experimental-traceological approach. Archaeol. Anthropol. Sci. 17, 30. https://doi.org/10.1007/s12520-024-02138-7.

Barbour, G.B., Licent, E., Teilhard de Chardin, P., 1926. Geological study of the deposits of the Sangkanho Basin. Bulletin of the Geological Society of China 5, 263–278.
Bavel, C. van, Thiels, W., Jelier, R., 2023. Cell shape characterization, alignment, and comparison using FlowShape. Bioinformatics 39 btad383.
Braun, D.R., Aldeias, V., Archer, W., Arrowsmith, J.R., Baraki, N., Campisano, C.J., Deino, A.L., DiMaggio, E.N., Dupont-Nivet, G., Engda, B., Feary, D.A., Garello, D.I., Kerfelew, Z., McPherron, S.P., Patterson, D.B., Reeves, J.S., Thompson, J.C., Reed, K. E., 2019. Earliest known Oldowan artifacts at >2.58 Ma from Ledi-Geraru, Ethiopia, highlight early technological diversity. Proc. Natl. Acad. Sci. 116, 11712–11717. https://doi.org/10.1073/pnas.1820177116.
Cabanès, J., Borel, A., Baena Preysler, J., Lourdeau, A., Cliquet, D., Colonge, D., Moncel, M.-H., 2024. Exploring the technological and functional diversity of polyhedrons, spheroids and bolas: an integrated and comparative analysis of cases from France and North Africa. Journal of Paleolithic Archaeology 7, 30. https://doi.org/10.1007/s41982-024-00195-x.
Cabanès, J., Borel, A., Baena Preysler, J., Lourdeau, A., Moncel, M.-H., 2022. Palaeolithic polyhedrons, spheroids and bolas over time and space. PLoS One 17, e0272135. https://doi.org/10.1371/journal.pone.0272135.
Cao, Y., Yi, M., Chen, F., Wang, H., 2025. Lithic variability and raw material exploitation strategies at Shuidonggou Locality 12, China: a quantitative approach. Archaeometry 67, 1515–1530. https://doi.org/10.1111/arcm.13106.
Clark, J.D., 1955. The stone ball: its associations and use by prehistoric man in Africa. In: Balout, L. (Ed.), II Congrès Panafricain de Préhistoire, Alger. Actes de La IIe Session. Arts et Métiers Graphiques, Paris, pp. 403–417.
Clarkson, C., 2013. Measuring core reduction using 3D flake scar density: a test case of changing core reduction at Klasies River Mouth, South Africa. J. Archaeol. Sci. 40, 4348–4357.
Dai, E., Xu, C., 1973. New Paleolithic materials and the Lantian Man culture. Kaogu Xuebao 1–12.
de la Torre, I., 2004. Omo revisited: evaluating the technological skills of Pliocene hominids. Curr. Anthropol. 45, 439–465. https://doi.org/10.1086/422079.
de la Torre, I., 2011. The Early Stone Age lithic assemblages of Gadeb (Ethiopia) and the Developed Oldowan/Early Acheulean in East Africa. J. Hum. Evol. 60, 768–812.
de la Torre, I., Mora, R., 2018. Oldowan technological behaviour at HWK EE (Olduvai Gorge, Tanzania). J. Hum. Evol. 120, 236–273.
de Weyer, L., 2017. An early Stone Age in Western Africa? Spheroids and polyhedrons at Ounjougou, Mali. Journal of Lithic Studies 4. https://doi.org/10.2218/jls.v4i1.1682.
Deng, C., Zhu, R., Zhang, R., Ao, H., Pan, Y., 2008. Timing of the Nihewan formation and faunas. Quat. Res. 69, 77–90.
Du, Y., Yue, Z., Zhi, Y., Shuwen, P., 2023. A taphonomic analysis of faunal remains from the Jijiazhuang Paleolithic site in the Yuxian Basin. Acta Anthropol. Sin. 42 (3), 359–372.
Duke, H., Feibel, C., Harmand, S., 2021. Before the Acheulean: the emergence of bifacial shaping at Kokiselei 6 (1.8 Ma), West Turkana, Kenya. J. Hum. Evol. 159, 103061.
Eerkens, J.W., Bettinger, R.L., 2001. Techniques for assessing standardization in artifact assemblages: can we scale material variability? Am. Antiq. 66, 493–504. https://doi.org/10.2307/2694247.
Fang, Y., Wang, J., Liang, R., Wang, J., Zhai, Z., Yang, C., 2002. Paleolithic artifacts discovered at Fangniushan, Jurong County, Jiangsu Province. Acta Anthropol. Sin. 21, 41–49.
Gallotti, R., Mussi, M., others, 2018. The Emergence of the Acheulean in East Africa and Beyond. Springer, Cham.
Grieb, J., Barbero-García, I., Lerma, J.L., 2022. Spherical harmonics to quantify cranial asymmetry in deformational plagiocephaly. Sci. Rep. 12, 167. https://doi.org/10.1038/s41598-021-04181-z.
Hallinan, E., Cascalheira, J., 2025. Quantifying Levallois: a 3D geometric morphometric approach to Nubian technology. Archaeol. Anthropol. Sci. 17. https://doi.org/10.1007/s12520-025-02199-2.
Harper, C.M., Goldstein, D.M., Sylvester, A.D., 2022. Comparing and combining sliding semilandmarks and weighted spherical harmonics for shape analysis. J. Anat. 240, 678–687.
Hewitt, M.N., Cruz, I.A., Linbo, T.H., Raible, D.W., 2024. Spherical harmonics analysis reveals cell shape-fate relationships in zebrafish lateral line neuromasts. Development 151 (2). https://doi.org/10.1242/dev.202251 dev202251.
Huang, W., 1964. Paleolithic artifacts from the Sanmenxia region in western Henan. Vertebr. Palasiat. 2, 66–85.
Inizan, M.-L., Reduron-Ballinger, M., Roche, H., 1999. Technology and Terminology of Knapped Stone, fifth ed. Cercle de Recherches et d'Études Préhistoriques, Nanterre.
Isaac, G.L., 1981. Stone Age visiting cards: approaches to the study of early landuse patterns. In: Hodder, I., Isaac, G., Hammond, N. (Eds.), Pattern of the Past: Studies in Honour of David Clarke. Cambridge University Press, Cambridge, pp. 131–155.
Isaac, G.L., 1986. Foundation stones: early artifacts as indicators of activities and abilities. In: Bailey, G.N., Callow, P. (Eds.), Stone Age Prehistory: Studies in Memory of Charles McBurney. Cambridge University Press, Cambridge, pp. 221–241.
Jia, L., 1959. A Paleolithic cultural site at Xigou, Licun, Quwo County, Shanxi Province. Kaogu (Archaeology) 1, 19–20.
Jia, L., 1962. Kehe: an Early Paleolithic Cultural Site in Southwestern Shanxi. Science Press, Beijing.
Jia, L., Wei, Q., Li, C., 1979. Excavation report of the Xujiayao Paleolithic cultural site in 1976. Vertebr. Palasiat. 4 (277–293), 347–350.
Jia, L., Wei, Q., 1976. The Paleolithic cultural site of Xujiayao, Yanggao. Kaogu Xuebao. Acta Archaeologica Sinica) 2, 97–114.
Jones, P.R., others, 1994. Results of experimental work in relation to the stone industries of Olduvai Gorge. Olduvai gorge 5, 1968–1971.
Kleindienst, M.R., 1962. Components of the East African Acheulean assemblage: an analytic approach. In: Actes Du IVeme Congres Panafricain de Préhistoire Et de l'étude Du Quaternaire. Musée royal de l'Afrique centrale Tervuren, pp. 81–105.
Kuman, K., Li, C., Li, H., 2014. Large cutting tools in the Danjiangkou Reservoir region, central China. J. Hum. Evol. 76, 129–153.
Leakey, M.D., 1971. Olduvai Gorge. In: Excavations in Beds I and II, vol. 3. Cambridge University Press, Cambridge, pp. 1960–1963.
Leakey, M.D., 1979. Olduvai Gorge: My Search for Early Man. William Collins, London.
Li, X., 2020. Paleoclimatic evidence inferred from soluble salt deposits in the Pleistocene sediments at Jijiazhuang site, Nihewan Basin. Mar. Geol. Quat. Geol. 40 (5), 149–159.
Li, H., Kuman, K., Li, C., 2018. What is currently (un)known about the Chinese Acheulean, with implications for hypotheses on the earlier dispersal of hominids. C. R. Palevol 17, 120–130.
Li, R., Qiao, J., Qiu, W., Zhai, Q., Li, Y., 2000. Soluble salt deposit in the Nihewan beds and its environmental significance. Sci. China Earth Sci. 43, 464–479.
Li, C., Xu, C., 1991. Paleolithic artifacts discovered at the Liao River in Anyi, Jiangxi, and their significance. Acta Anthropol. Sin. 10 (1), 34–41.
Lin, S.C., 2024. A new method for quantifying flake scar organisation on cores using orientation statistics. J. Archaeol. Sci. 167, 105998.
Link, R., Jaggy, M., Bastmeyer, M., Schwarz, U.S., 2024. Modelling cell shape in 3D structured environments: a quantitative comparison with experiments. PLoS Comput. Biol. 20, e1011412.
Liu, Y., Huang, W., Lin, Y., 1984. Human fossils and Paleolithic artifacts discovered in Jingchuan, Gansu Province. Acta Anthropol. Sin. 3 (1), 11–18.
Lixian County Museum, 1992. A brief report on the Paleolithic localities at Zhangjiatan and Xiangong in Lixian, Hunan Province. Huaxia Archaeology 4, 1–8.
Lu, L., Dong, B., Chen, S., 2021. An experimental study on stone spheroids from the Paleolithic period in China. Acta Anthropol. Sin. 40 (4), 13.
Lu, N., , Chinese Academy of Sciences, of the, G.S., Hou, Y., 2006. Analysis and comparative study of lithic manufacturing patterns at the Liangshan site. In: Annual Meeting of the Vertebrate Paleontology Section. Palaeontological Society of China.
Lycett, S.J., Von Cramon-Taubadel, N., 2013. A 3D morphometric analysis of surface geometry in Levallois cores: patterns of stability and variability across regions and their implications. J. Archaeol. Sci. 40, 1508–1517. https://doi.org/10.1016/j.jas.2012.11.005.
Ma, N., Pei, S., Gao, X., 2011. Study of lithic artifacts excavated from Locality 74093 at the Xujayao site in 1977. Acta Anthropol. Sin. 30 (3), 275–288.
Medyukhina, A., Blickensdorf, M., Cseresnyés, Z., Ruef, N., Stein, J.V., Figge, M.T., 2020. Dynamic spherical harmonics approach for shape classification of migrating cells. Sci. Rep. 10, 6072.
Mora, R., de La Torre, I., 2005. Percussion tools in Olduvai Beds I and II (Tanzania): implications for early human activities. J. Anthropol. Archaeol. 24, 179–192. https://doi.org/10.1016/j.jaa.2004.12.001.
Muller, A., Barsky, D., Sala-Ramos, R., Sharon, G., Titton, S., Vergès, J.-M., Grosman, L., 2023. The limestone spheroids of 'Ubeidiya: intentional imposition of symmetric geometry by early hominins? R. Soc. Open Sci. 10, 230671.
Muller, A., Clarkson, C., 2023. Filling in the blanks: standardization of lithic flake production throughout the Stone Age. Lithic Technol. 48, 222–236. https://doi.org/10.1080/01977261.2022.2103290.
Mussi, M., 2025. The volcanic rock spheres of Melka Kunture (Upper Awash, Ethiopia) at Gombore IB and later Acheulean sites. Quat. Int. 721, 109681. https://doi.org/10.1016/j.quaint.2025.109681.
Nanjing Institute of Geology and Palaeontology, Chinese Academy of Sciences, 1985. Palaeontologia Sinica, Whole Volume No. 168, New Series d, No. 12: a Study of Peking Man's Lithic Artifacts. Science Press.
Noshita, K., Nakagawa, T., Kaneda, A., Tamura, K., Nakao, H., 2025. The cultural transmission of Ongagawa style pottery in the prehistoric Japan: quantitative analysis on three-dimensional data of archaeological pottery in the early Yayoi period. J. R. Soc. Interface 22, 20240889.
Pei, S., Wang, F., Niu, D., 2024. A general review on the discovery and research progress of hominins in the Nihewan Basin since the 21st century. Acta Anthropol. Sin, 43 (06), 913-933.
Pei, S., Deng, C., La Torre, I. de, Jia, Z., Ma, D., Li, X., Wang, X., 2019. Magnetostratigraphic and archaeological records at the Early Pleistocene site complex of Madigou (Nihewan Basin): implications for human adaptations in North China. Palaeogeogr. Palaeoclimatol. Palaeoecol. 530, 176–189. https://doi.org/10.1016/j.palaeo.2019.05.014.
Pei, S., Ma, D., Jia, Z., Li, X., Wang, X., Wang, F., Yang, H., 2018. A preliminary report on excavation of the Jijiazhuang Paleolithic site in the Yuxian Basin, North China. Acta Anthropol. Sin. 37, 510–528.
Pei, S., Xie, F., Deng, C., Jia, Z., Wang, X., Guan, Y., Li, X., Ma, D., La Torre, I. de, 2017. Early Pleistocene archaeological occurrences at the Feiliang site, and the archaeology of human origins in the Nihewan Basin, North China. PLoS One 12, e0187251. https://doi.org/10.1371/journal.pone.0187251.
Pei, S., Hou, Y., 2002. Preliminary study on raw materials exploitation at Donggutuo site, Nihewan Basin, North China. Acta Anthropol. Sin. Suppl. l. 21, 53–66.
Sahnouni, M., Schick, K., Toth, N., 1997. An experimental investigation into the nature of faceted limestone "Spheroids" in the Early Palaeolithic. J. Archaeol. Sci. 24, 701–713. https://doi.org/10.1006/jasc.1996.0152.
Schick, K.D., Toth, N., 1994. Early Stone Age technology in Africa: a review and case study into the nature and function of spheroids and subspheroids. In: Corruccini, R. S., Ciochon, R.L. (Eds.), Integrative Paths to the Past: Paleoanthropological Advances in Honor of f. Clark Howell. Prentice Hall, New Jersey, pp. 429–449.

Shanxi Provincial Institute of Archaeology, 2014. The Dingcun Paleolithic Site Complex: Excavation Report of the Dingcun Sites (1976–1980). Cultural Relics Publishing House.
Sholts, S.B., Gingerich, J.A., Schlager, S., Stanford, D.J., Wärmländer, S.K., 2017. Tracing social interactions in Pleistocene North America via 3D model analysis of stone tool asymmetry. PLoS One 12, e0179933.
Tan, Y., 1999. A report on the Paleolithic locality on the northern slope of Huzhua Mountain. Hunan Archaeological Journal 15.
Tao, F., Liang, Z., Xie, X., Yin, Z., Ding, W., Hu, W., Ding, S., Yang, F., Yin, L., Xie, X., 1984. Excavation Report of Locality 80:01 at the Dingcun Paleolithic Site. Prehistoric Research, pp. 57–68.
Texier, P.-J., Roche, H., 2014. Polyèdre, sub-sphéroïde, sphéroïde et bola: des segments plus ou moins longs d'une même chaîne opératoire. Cahier noir 31–40.
Titton, S., Barsky, D., Bargalló, A., Serrano-Ramos, A., Vergès, J.M., Toro-Moyano, I., Sala-Ramos, R., Solano, J.G., Arenas, J.M.J., 2020. Subspheroids in the lithic assemblage of Barranco León (Spain): recognizing the late Oldowan in Europe. PLoS One 15, e0228290. https://doi.org/10.1371/journal.pone.0228290.
Vaquero, M., Romagnoli, F., 2018. Searching for lazy people: the significance of expedient behavior in the interpretation of Paleolithic assemblages. J. Archaeol. Method Theor 25, 334–367. https://doi.org/10.1007/s10816-017-9339-x.
Wadell, H., 1935. Volume, shape, and roundness of quartz particles. J. Geol. 43, 250–280. https://doi.org/10.1086/624298.
Wang, F., 2016. Comprehensive Study of the Houjiayao Site. Hebei Normal University. Ph.D. dissertation.
Wang, S., Sun, X., Lu, H., Yi, S., Zhang, G., Xing, L., Zhuo, H., Yu, K., Wang, W., 2014. Newly discovered Paleolithic artifacts and their chronology in the upper Han River and Hanzhong Basin. Acta Anthropol. Sin. 33 (2), 125–136.
Wang, S., Zhang, X., Lu, H., et al., 2013. Newly discovered Paleolithic artifacts and their buried loess strata in the Shangdan Basin, Upper Danjiang River. Acta Anthropol. Sin. 32, 421–431.
Wang, X., Wei, J., Chen, Q., Tang, Z., Wang, C., 2010. Excavation report of the Jinstai Cave site, Inner Mongolia. Acta Anthropol. Sin. 29 (1), 15–32.
Wang, S., Hu, S., 2000. Paleolithic artifacts from the Yaoshi Basin, Upper Danjiang River. Kaogu yu Wenwu (Archaeology and Cultural Relics) 4, 36–42.
Wei, Q., Huang, W., Zhang, X., 1984. Newly discovered Paleolithic artifacts at Mujiaqiao, Lijiang. Acta Anthropol. Sin. 3 (3), 225–236.
Wieczorek, M.A., Meschede, M., 2018. SHTools: tools for working with spherical harmonics. G-cubed 19, 2574–2592.
Willoughby, P.R., 1985. Spheroids and battered stones in the African Early Stone Age. World Archaeol. 17, 44–60. https://doi.org/10.1080/00438243.1985.9979949.
Wu, Z., Sun, B., 1989. Preliminary study of the Paleolithic cave site complex at Dangcheng, Heshun County, Shanxi Province. Acta Anthropol. Sin. 8 (1), 39–48, 102.
Xi, D., 1994. A report on the Paleolithic survey in the lower reaches of the Yuan River. Hunan Archaeological Journal 6.
Xia, W., Wang, S., Wang, X., Lu, H., Xia, N., Zhang, G., Bie, J., Yang, X., Wu, J., 2022. A study of the lithic artifacts from the Paleolithic locality at Fanba, Yangxian, Hanzhong Basin. Acta Anthropol. Sin. 41 (3), 381–393.
Xiaokongshan Joint Excavation Team, 1988. Excavation report of the Xiaokongshan Paleolithic site in Nanzhao, Henan, in 1987. Huaxia Archaeology 4, 1–15.
Xie, J., 1982. The Paleolithic site at Liujiacha, Huan County, Gansu Province. Kaogu Xuebao Acta Archaeologica Sinica 1, 35–48.
Yang, S., Hou, Y., Pelegrin, J., 2016. A late Acheulean culture on the Chinese Loess Plateau: the techno-economic behavior of the Dingcun lithic industry. Quat. Int. 400, 73–85.
Yang, S., Petraglia, M.D., Hou, Y.-M., Yue, J., Deng, C., Zhu, R., 2017. The lithic assemblages of Donggutuo, Nihewan Basin: knapping skills of early Pleistocene hominins in North China. PLoS One 12, e0185101. https://doi.org/10.1371/journal.pone.0185101.
Yang, S.-X., Deng, C.-L., Zhu, R.-X., Petraglia, M.D., 2020. The Paleolithic in the Nihewan Basin, China: evolutionary history of an early to late Pleistocene record in Eastern Asia. Evol. Anthropol. Issues News Rev. 29, 125–142. https://doi.org/10.1002/evan.21813.
Ye, Z., Lin, S., Marwick, B., 2025a. Workflow for Marking and Exporting Lithic Scar Orientations Using Geomagic Wrap and Rhino. https://doi.org/10.17504/protocols.io.rm7vz1dj8lx1/v1. https://www.protocols.io/.
Ye, Z., Pei, S., Ma, D., Jia, Z., Wang, F., Yang, H., 2025b. Preliminary report on the excavation of Qianshangying-B Paleolithic site at Yuxian in the Nihewan Basin. Acta Anthropol. Sin. 44. https://doi.org/10.16359/j.1000-3193/AAS.2025.0109.
Ye, Z., Pei, S., Tu, H., Du, Y., Ma, D., Li, H., Xu, J., Luo, L., Lai, Z., Granger, D., others, 2024. 26Al/10Be burial dating and technological strategies of hominins at the Jijiazhuang Paleolithic site, Nihewan Basin, China: implications for understanding Middle Pleistocene human adaptations in East Asia. Quat. Sci. Rev. 339, 108837.
Yi, M., Gao, X., Pei, S., 2012. A preliminary analysis of the definition, classification, and function of stone spheroids. Acta Anthropol. Sin. 31 (4), 355–363.
Yuan, B., Tong, H., Wen, R., Wang, Y., 2009. The formation mechanism of the Nihewan paleo-lake and its relationship with living environment for early ancient human. J. Geomechanics 15, 77–87.
Zhou, T., Li, H., Liu, Q., Li, R., Sun, X., 1991. Study on the Cenozoic paleogeograpgy of Nihewan Basin. Science, Beijing (in Chinese).
Zhu, R.X., Hoffman, K.A., Potts, R., Deng, C.L., Pan, Y.X., Guo, B., Shi, C.D., Guo, Z.T., Yuan, B.Y., Hou, Y.M., Huang, W.W., 2001. Earliest presence of humans in Northeast Asia. Nature 413, 413–417. https://doi.org/10.1038/35096551.
Zhu, R.X., Potts, R., Xie, F., Hoffman, K.A., Deng, C.L., Shi, C.D., Pan, Y.X., Wang, H.Q., Shi, R.P., Wang, Y.C., Shi, G.H., Wu, N.Q., 2004. New evidence on the earliest human presence at high northern latitudes in Northeast Asia. Nature 431, 559–562. https://doi.org/10.1038/nature02829.